Article

Immunity

Renal NF-κB activation impairs uric acid homeostasis to promote tumor-associated mortality independent of wasting

Graphical abstract

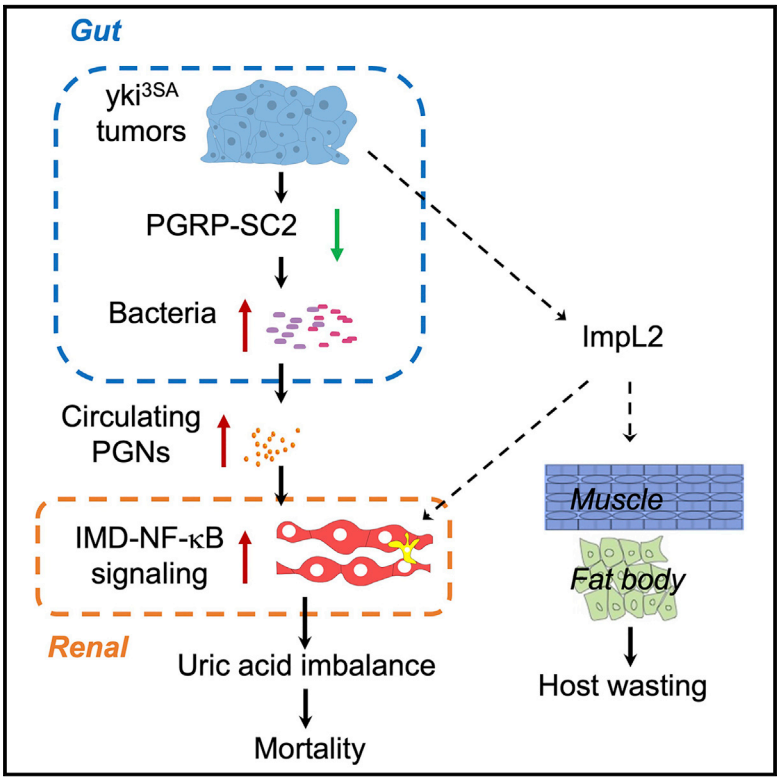

Authors

Yuchen Chen, Wenhao Xu, Yuan Chen, Anxuan Han, Jiantao Song, Xiaoya Zhou, Wei Song

Correspondence

songw@whu.edu.cn

In brief

How host immune responses contribute to tumor-associated wasting or mortality is unknown. Chen et al. show that *Drosophila* yki^{3SA}-gut tumors suppress PGRP-SC2 production to cause gut bacterial overload and systemic IMD-NF-κB activation, promoting host death without affecting wasting. They demonstrate that renal IMD-NF-κB-mediated uric acid accumulation increases host mortality.

Highlights

- Fly yki^{3SA}-gut tumors cause bacterial overload via suppression of gut PGRP-SC2
- Gut bacterial clearance increases survival of yki^{3SA}-tumor-bearing flies
- Renal-specific IMD-NF-κB blockade increases survival of yki^{3SA}-tumor-bearing flies
- Renal IMD-NF-κB blockade diminishes yki^{3SA}-tumor-associated uric acid accumulation

Chen et al., 2022, Immunity *55*, 1–15
September 13, 2022
https://doi.org/10.1016/j.immuni.2022.07.022

CellPress

Immunity

CellPress

Article

Renal NF-κB activation impairs uric acid homeostasis to promote tumor-associated mortality independent of wasting

Yuchen Chen,[1,2] Wenhao Xu,[1,2] Yuan Chen,[1,2] Anxuan Han,[1,2] Jiantao Song,[1,2] Xiaoya Zhou,[1,2] and Wei Song[1,2,3,*]
[1]Department of Hepatobiliary and Pancreatic Surgery, Frontier Science Center for Immunology and Metabolism, Medical Research Institute, Zhongnan Hospital of Wuhan University, Wuhan University, Wuhan, Hubei 430071, China
[2]TaiKang Center for Life and Medical Sciences, Wuhan University, Wuhan, Hubei 430071, China
[3]Lead contact
*Correspondence: songw@whu.edu.cn
https://doi.org/10.1016/j.immuni.2022.07.022

SUMMARY

Tumor-induced host wasting and mortality are general phenomena across species. Many groups have previously demonstrated endocrinal impacts of malignant tumors on host wasting in rodents and *Drosophila*. Whether and how environmental factors and host immune response contribute to tumor-associated host wasting and survival, however, are largely unknown. Here, we report that flies bearing malignant yki^{3SA}-gut tumors exhibited the exponential increase of commensal bacteria, which were mostly acquired from the environment, and systemic IMD-NF-κB activation due to suppression of a gut antibacterial amidase PGRP-SC2. Either gut microbial elimination or specific IMD-NF-κB blockade in the renal-like Malpighian tubules potently improved mortality of yki^{3SA}-tumor-bearing flies in a manner independent of host wasting. We further indicate that renal IMD-NF-κB activation caused uric acid (UA) overload to reduce survival of tumor-bearing flies. Therefore, our results uncover a fundamental mechanism whereby gut commensal dysbiosis, renal immune activation, and UA imbalance potentiate tumor-associated host death.

INTRODUCTION

Cancer cachexia, or tumor-induced host wasting, is a process characterized by body weight loss, atrophy of skeletal and adipose tissue, hyperglycemia, and mortality (Fearon et al., 2013; Tisdale, 2002). Due to the unclear pathogenic mechanisms, different model organisms from rodents to *Drosophila* have been used to mimic the wasting development and address the unmet clinical needs. Recent studies using tumor-bearing mice have demonstrated the cachectic roles of circulating secreted proteins, such as activins, myostatin, transforming growth factor β (TGF-β), parathyroid hormone-related protein (PTHrP), interleukin-6 (IL-6), IL-1, tumor necrosis factor α (TNF-α), and interferon γ (IFN-γ), in mediating host organ wasting in response to tumor growth (Ballaro et al., 2016; Baracos et al., 2018). However, most of these mice studies were performed in specific-pathogen-free (SPF) conditions and ignored the potential participation of environmental microorganisms such as bacteria, fungi, and viruses that inevitably interact with the host to modulate host immune response and physiological outputs. Whether and how environmental factors and host immune response contribute to tumor-induced organ wasting or mortality are largely unknown.

Drosophila has emerged as an evolutionarily conserved model organism to investigate the mechanism of cancer cachexia in the past years. We have established that induction of an active transcription factor *yki^{3SA}*, a homolog of the human oncogene YAP1, in intestinal stem cells (ISCs) leads to overproliferation of gut tumor cells and subsequent wasting phenotypes, including muscle dysfunction, lipid loss, hyperglycemia, and mortality (Kwon et al., 2015). We further characterized the molecular mechanisms through which malignant yki^{3SA}-gut-tumor cells produce cachectic ligands, including ImpL2, Pvf1, and Upd3, to remotely impair anabolism-catabolism balance in host organs via modulation of insulin, MEK, and Jak/Stak signaling pathways, causing wasting phenotypes (Ding et al., 2021; Kwon et al., 2015; Song et al., 2019). Other groups using different tumor models in *Drosophila* and mice also observe similar cachectic roles of tumor-secreted proteins in the wasting development (Dong et al., 2021; Figueroa-Clarevega and Bilder, 2015; Kandarian et al., 2018; Newton et al., 2020; Nie et al., 2019; Yeom et al., 2021). These findings collectively demonstrate that tumor-induced wasting is a general phenomenon and that *Drosophila* can be used to dissect the molecular mechanisms involved in tumor-host interaction. Moreover, different from SPF mice, tumor-bearing flies are cultured at a less-restricted condition with direct interaction with natural air and external microorganisms and provide a convenient tool to investigate microbial-host interaction in the context of malignant tumor growth.

Drosophila has also emerged as an excellent model to conduct genetic analysis of microbial recognition, immune

Please cite this article in press as: Chen et al., Renal NF-κB activation impairs uric acid homeostasis to promote tumor-associated mortality independent of wasting, Immunity (2022), https://doi.org/10.1016/j.immuni.2022.07.022

defense, and host physiological perturbation (Buchon et al., 2014; Capo et al., 2019; Charroux and Royet, 2012; Lee and Brey, 2013) due to the simpler gut commensal communities and conserved immune regulation. Two innate immune NF-κB pathways, Toll and immune deficiency (IMD), have been identified as the major signaling cascades to regulate the humoral reactions in response to the diverse bacteria and fungi (Lemaitre and Hoffmann, 2007). The Toll-NF-κB signaling is triggered by Gram-positive bacterial Lysine-type peptidoglycans (PGNs) and fungal β-(1,3)-glucan via binding to peptidoglycan recognition proteins (PGRPs) and glucan-binding proteins (GNBPs), respectively, to cleave cytokine Spaetzle (Spz) and activate Toll receptor as well as the Dorsal-Dif transcriptional complex (Ferrandon et al., 2007). On the other hand, Gram-negative bacterial DAP-type PGNs trigger IMD-NF-κB signaling through interaction with PGRP-LC to activate IMD and the downstream transcriptional factor Relish (Rel) (Ferrandon et al., 2007). A subgroup of PGRPs, such as PGRP-LB with the amidase enzymatic activity, have been found to degrade PGNs and suppress the immune responses upon infection (Charroux et al., 2018; Zaidman-Remy et al., 2006). Activated Toll and IMD pathways in multiple tissues like gut and fat body induce expression of anti-microbial peptide (AMP) genes such as *Drosomycin* (*Drs*) and *Diptericin* (*Dpt*), respectively, and others to restrain the microbial growth in a feedback loop (Lemaitre and Hoffmann, 2007; Royet and Dziarski, 2007). In addition, activation of NF-κB pathways in *Drosophila* also involves regulation of energy balance and host death (Buchon et al., 2014; Garschall and Flatt, 2018; Molaei et al., 2019), the major features of tumor-induced host wasting or mortality. It raises a hypothesis whereby systemic immune response plays pathogenic roles in the context of tumor growth.

In this study, we observed a robust systemic activation of IMD-NF-κB signaling in yki^{3SA}-tumor bearing flies due to suppressed production of gut PGRP-SC2, a key antibacterial amidase characterized by us, and increased abundance of commensal bacteria. We found that bacteria-induced IMD-NF-κB activation in the renal organ impaired UA metabolism to decrease survival of yki^{3SA} flies without affecting tumor growth or energy wasting. Thus, our results indicate that gut-microbial dysbiosis and renal-IMD-NF-κB activation promote mortality independent of host wasting in yki^{3SA}-tumor-bearing flies.

RESULTS

yki^{3SA}-tumor-bearing flies exhibit systemic activation of IMD-NF-κB signaling and gut microbial overload

In a previous study, our RNA sequencing (RNA-seq) data have shown that AMP-encoding genes are up-regulated in the muscle of yki^{3SA}-tumor-bearing flies compared with control flies (Figure 1A; Ding et al., 2021). qPCR analysis in whole flies also showed that mRNA amounts of AMPs downstream IMD-NF-κB signaling such as *DptA*, *DptB*, *AttA*, *AttD*, but not Toll-NF-κB signaling like *Drs*, were increased by >10-fold (Figure 1B), suggesting the activation of systemic IMD-NF-κB signaling in yki^{3SA} flies. As microbiota and their cell-wall PGNs act as the key elicitors of immune response and induce the expression of AMPs in *Drosophila* (Royet and Dziarski, 2007), we detected overall microbial load in the gut and found a >500-fold increase in yki^{3SA} flies (Figure 1C). We also observed an increase of circulating PGNs in the hemolymph of yki^{3SA} flies compared with control flies using a silkworm larvae plasma (SLP) kit (Figure 1D). These results indicate that yki^{3SA}-gut tumors cause an exponential microbial increase in the gut and systemic IMD-NF-κB activation.

To further explore the change of the gut microbiota in yki^{3SA} flies, we performed metagenomics sequencing using gut DNA isolated from yki^{3SA} and control flies (GSE204975) (Figure S1A). We observed an increase of general microbial abundance and perturbed composition in the yki^{3SA} guts (Figure 1E and Table S1). For example, the abundances of most Gram-negative bacteria, including the major commensal such as *Acetobacter*, *Gluconobacter*, *Komagataeibacter*, and *Pseudomonas* species, were increased in the yki^{3SA} guts (Figures 1E and S1A). Gram-positive bacteria *Lactobacillus*, fungi like *Pochonia*, as well as others, were also increased in the yki^{3SA} guts (Figures 1E and S1A). In contrast, yki^{3SA} guts exhibited the decreased abundance of certain commensal microbiota (Figures 1E and S1A). These results demonstrate that yki^{3SA}-tumor-bearing flies exhibit a great overload of gut microbiota with perturbed composition.

Gut microbial elimination alleviates tumor-induced IMD-NF-κB activation and host death

Fly immune responses and NF-κB signaling regulate multiple biological processes beyond AMP expression such as lipid metabolism, development, and aging (Buchon et al., 2014; Petkau et al., 2017; Zhou and Boutros, 2020). We wondered whether the gut microbial increase contributes to yki^{3SA} tumor-induced wasting or mortality. To test this hypothesis, we first eliminated the microbiota in adult flies by feeding antibiotics (Abs) in the food after the virgin eclosion. The microbiota could barely be detected in yki^{3SA} flies after antibiotic treatment (Figure 1C). As expected, we found that mRNA induction of AMPs like *DptA*, *DptB*, *AttA*, *AttD*, but not *Drs*, was suppressed (Figure 1B), indicating the specific blockade of IMD-NF-κB, but not Toll-NF-κB, signaling. Antibiotic treatment failed to affect growth of tumor cells labeled by GFP or bloating phenotypes of yki^{3SA} flies (Figure 1F). However, yki^{3SA} tumor-induced mortality was alleviated with a ~25% increase in the median lifespan (Figure 1G). To confirm the effects of microbial elimination, we made tumor-bearing flies germ free (GF) using a sodium hypochlorite-based method (Ryu et al., 2008). The systemic IMD-NF-κB activation was also blunted (Figure 1I). Again, we observed an increase of survival but no changes in tumor growth or abdomen bloating of germ-free yki^{3SA} flies (Figures 1H and 1J). These results demonstrate that yki^{3SA}-gut-bearing tumors trigger, at least, gut microbial growth and systemic IMD-NF-κB activation to promote host death.

Gut microbiota elimination does not affect tumor-induced host wasting

We wondered whether gut microbiota also contribute to yki^{3SA}-tumors-associated host wasting. To address this hypothesis, we examined the expression amounts of tumor-secreted cachectic ligands, including *ImpL2*, *Pvf1*, and *Upd3*, that cause host wasting and found that antibiotic treatment did not affect the expression of any of them (Figure 2A). In addition, antibiotic treatment failed to affect the tumor-induced host wasting, including abdominal bloating, hyperglycemia, climbing defect, and muscle mitochondrial injury, as indicated by fragmented

Please cite this article in press as: Chen et al., Renal NF-κB activation impairs uric acid homeostasis to promote tumor-associated mortality independent of wasting, Immunity (2022), https://doi.org/10.1016/j.immuni.2022.07.022

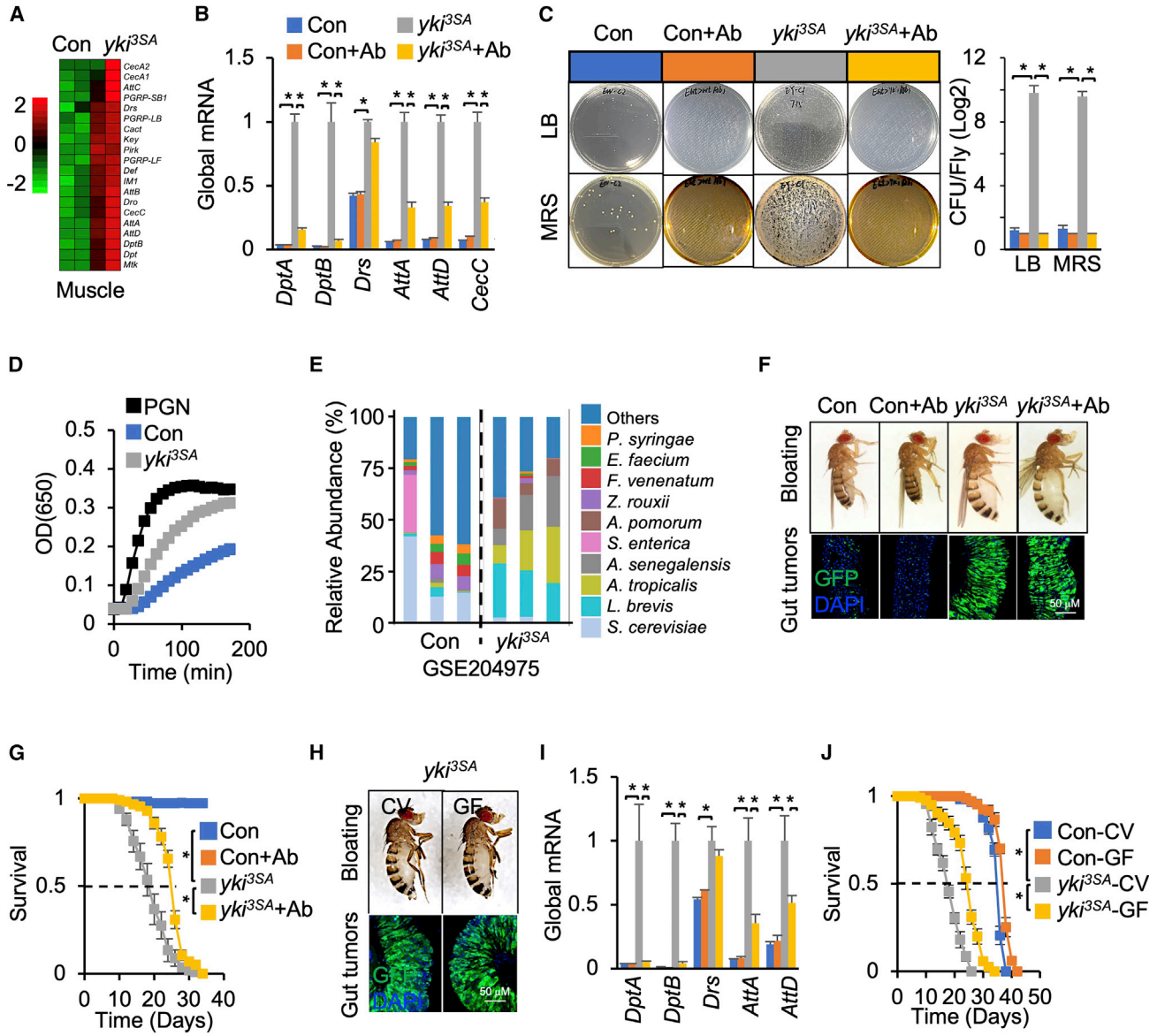

Figure 1. Gut microbial elimination suppresses IMD-NF-κB activation and improves mortality of yki^{3SA}-tumor-bearing flies

(A) Heatmap showing up-regulated genes that are related to immune response in the muscle of Con and *yki^{3SA}* flies after tumor induction for 8 days.

(B–F) Whole-body qPCR analysis of immune-associated gene expression (B, n = 6, 5 flies/replicate), gut bacterial loads determined by colonization on LB and MRS agar plates (left, bacterial images; right, quantification, n = 3, 5 flies/replicate) (C), hemolymph PGN amounts from 100 female adults indicated by enzyme kinetics using 100 ng/μL PGN as a positive control (D), top 10 species of gut microbiota indicated by metagenome sequencing analysis (E), bloating phenotypes (up) and gut tumors (bottom, GFP) (F) of flies under yki^{3SA}-tumor induction for 8 days using *GAL4* system with or without antibiotics treatment.

(G) Longevities of indicated flies (n = 120) (Log rank test, Con versus *yki^{3SA}*, $p < 0.001$; *yki^{3SA}* versus *yki^{3SA}* + Ab, $p < 0.001$).

(H–I) Abdomen bloating (up) and gut tumors (bottom, GFP) (H) and whole-body qPCR analysis of immune-associated gene expression (I, n = 6, 5 flies/replicate) of conventional (CV) or germ-free (GF) flies under yki^{3SA}-tumor induction for 8 days.

(J) Longevities of indicated flies (n = 120) (Log rank test, Con-CV versus *yki^{3SA}*-CV, $p < 0.001$; *yki^{3SA}*-CV versus *yki^{3SA}*-GF, $p < 0.001$).

(B, C, D, G, I, and J) Data are representative of at least three independent experiments. Data are presented as mean ± SEM Student's *t* test; *$p < 0.05$. "ns" indicates statistically non-significant. See also Figure S1 and Table S1.

cristae (C) and low-density inner space (S), and ovary atrophy, except that lipid loss was somehow alleviated (Figures 2B–2G). We did not observe obvious improvements in wasting in germ-free yki^{3SA} flies either (Figure 2H). Taken together, our results indicate that gut microbial increase and systemic IMD-NF-κB activation do not affect yki^{3SA}-tumors-induced host wasting.

yki^{3SA} tumors cause bacterial increase via suppression of gut PGRP-SC2

We next investigated how yki^{3SA}-gut-bearing tumors result in the exponential increase of microbiota. Fly midgut produces a series of PGRPs including PGRP-SB1, PGRP-SB2, PGRP-SC1a, PGRP-SC1b, and PGRP-SC2 that are predicted to cleave

Please cite this article in press as: Chen et al., Renal NF-κB activation impairs uric acid homeostasis to promote tumor-associated mortality independent of wasting, Immunity (2022), https://doi.org/10.1016/j.immuni.2022.07.022

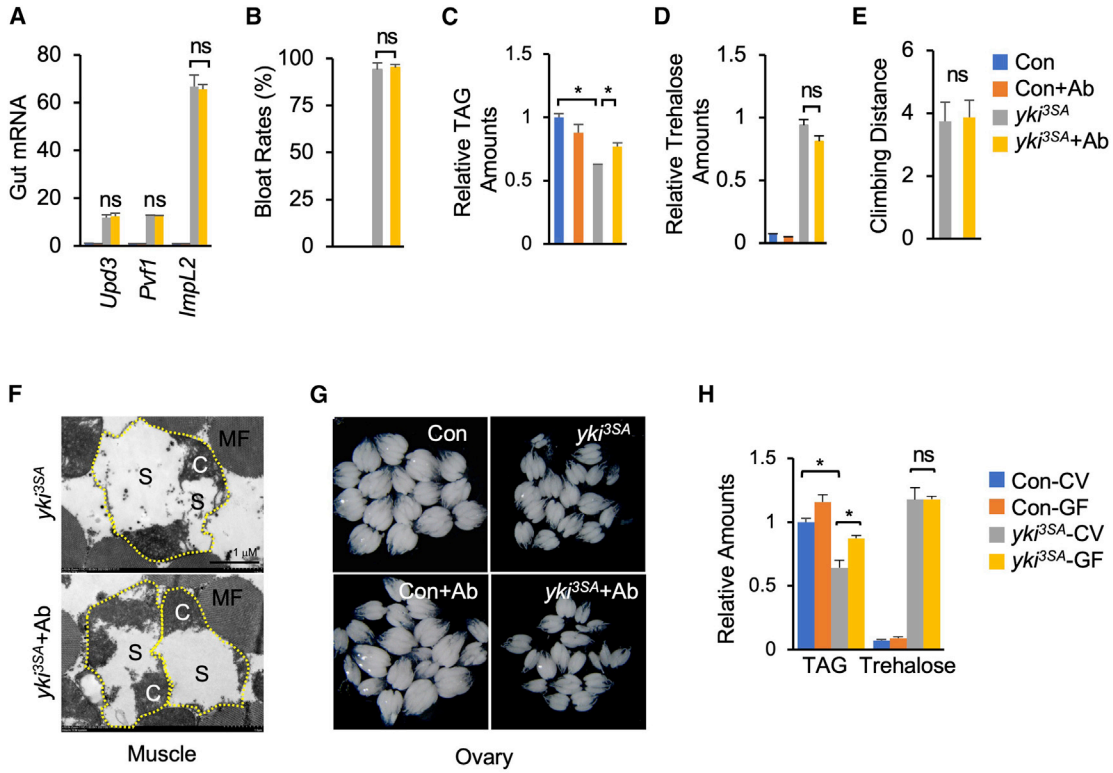

Figure 2. Gut microbial elimination does not rescue organ wasting of yki^{3SA}-tumor-bearing flies

(A–G) Gut qPCR analysis of tumor-derived cachectic ligands (A, n = 4, 10 flies/replicate), bloating rates (B, n = 4, 20 flies/replicate), TAG (C) and trehalose amounts (D, n = 4, 5 flies/replicate), climbing defects (E, n = 20), morphologies of injured mitochondria with fragmented cristae (C) and blank space (S) next to myofibrils (MF) (F), and ovary degeneration (G) of flies under yki^{3SA}-tumor induction for 8 days with or without antibiotics treatment.

(H) TAG and trehalose amounts (n = 3, 5 flies/replicate) of conventional (CR) or germ-free (GF) flies under yki^{3SA}-tumor induction for 8 days.

(A–E and H) Data are representative of at least three independent experiments. Data are presented as mean ± SEM Student's *t* test; *p < 0.05. "ns" indicates statistically non-significant.

PGNs with putative amidase activities and maintain gut-microbial homeostasis (Costechareyre et al., 2016; Mellroth et al., 2003; Paredes et al., 2011). We hypothesized that microbial increase in yki^{3SA} guts is driven by suppression of certain amidase PGRPs. To test this hypothesis, we analyzed the expression of all PGRPs in yki^{3SA} guts. The RNA-seq data indicated that only *PGRP-SC1a*, *PGRP-SC1b*, and *PGRP-SC2* were suppressed in yki^{3SA} guts (Figure 3A). We also confirmed these results with qPCR analysis (Figure 3B). *PGRP-SC1a* and *PGRP-1b* express an identical transcript and protein, so we collectively named them as *PGRP-SC1*. Further, antibiotic treatment did not change yki^{3SA}-tumor-associated suppression of *PGRP-SC1 or PGRP-SC2* in the guts (Figure 3B). We also noticed that expressions of most marker genes of enterocytes (ECs) that produce PGRP-SC1 and PGRP-SC2 were decreased in the yki^{3SA} guts (Figures S1B–S1C). Taken together with decreased composition of ECs in yki^{3SA}-tumor guts (Figure 1F), our results suggest that yki^{3SA} induction in ISCs impairs general EC differentiation to decrease production of *PGRP-SC1* and *PGRP-SC2* in the gut.

To determine which PGRPs are essential for yki^{3SA}-tumor-induced microbial increase, we restored the expression of PGRP-SC1 or PGRP-SC2 in yki^{3SA}-tumor-bearing guts. We found that overexpression of PGRP-SC2, but not PGRP-SC1, completely abolished the elevation of gut bacteria and restored them to the abundances in control guts without affecting the gut-tumor growth (Figures 3C and 3D). PGRP-SC2 overexpression consistently decreased circulating PGN concentrations in the hemolymph and systemic expression of IMD-NF-κB target genes (Figures 3E and 3F). Importantly, overexpression of PGRP-SC2, but not PGRP-SC1, potently increased survival rates of yki^{3SA} flies (Figure 3G). These results demonstrate that yki^{3SA}-gut tumors impair intestinal PGRP-SC2 production to cause bacterial increase and host death.

We also investigated the roles of PGRP-SC2 in normal flies without tumors. To do this, we silenced *PGRP-SC2* expression in the ECs of control adult midguts using shRNAs driven by a temperature-sensitive *Myo1A-GAL4* (*Myo1A^{TS}*) and observed an increase in both systemic expression of IMD-NF-κB target genes and bacterial load at day 10 (Figures 4A–4C). Subsequently, the survival rates of flies with gut *PGRP-SC2* deficiency were significantly decreased compared with control flies (Figure 4D). We examined the role of gut PGRP-SC2 in pathogen infection as well as silenced *PGRP-SC2* expression in the control midguts using *Myo1A^{TS}* prior to oral *Ecc15* infection. Compared with *Ecc15*-induced systemic expression of IMD-NF-κB target genes and mortality in control flies, a higher induction of IMD-NF-κB target gene expression and mortality in flies with gut *PGRP-SC2* deficiency was observed. (Figures S1D–S1E). These

Please cite this article in press as: Chen et al., Renal NF-κB activation impairs uric acid homeostasis to promote tumor-associated mortality independent of wasting, Immunity (2022), https://doi.org/10.1016/j.immuni.2022.07.022

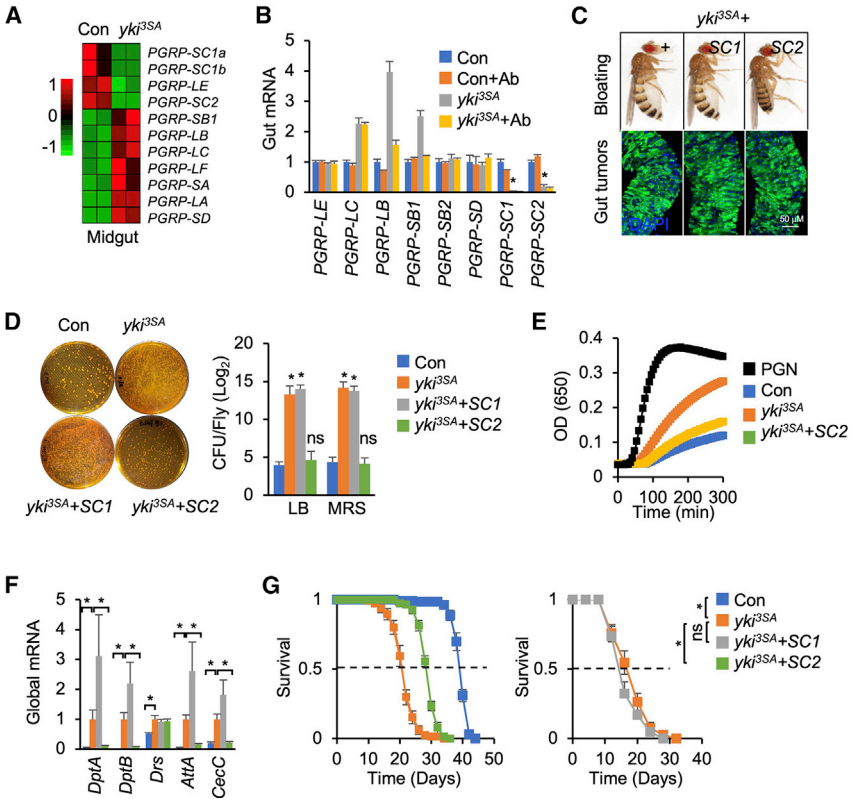

Figure 3. yki^{3SA} tumors unleash gut bacterial growth and activate IMD-NF-κB signaling via PGRP-SC2 suppression

(A and B) Heatmap of RNA-seq (A) and qPCR (B, n = 3, 10 flies/replicate) results showing differentially regulated genes of PGRP family in the gut of flies under tumor induction for 8 days with or without antibiotics treatment.

(C–F) Abdomen bloating (up) and gut tumors (bottom, GFP) (C), bacterial loads (D, left) and the quantification (D, right, n = 4, 5 flies/replicate), circulating PGN amounts from 100 adult females indicated by enzyme kinetics (E) and whole-body qPCR analysis of immune genes (F, n = 6, 5 flies/replicate) of flies under yki^{3SA}-tumor induction with PGRP-SC1 or PGRP-SC2 overexpression for 8 days (G) Lifespans of indicated flies (n = 120) (Log rank test, Con versus *yki^{3SA}*, $p < 0.001$; *yki^{3SA}* versus *yki^{3SA} + SC2*, $p < 0.001$).

(B, D, and E–G) Data are representative of at least three independent experiments. Data are presented as mean ± SEM Student's *t* test; *p < 0.05. "ns" indicates statistically non-significant. See also Figure S1.

results confirm the role of PGRP-SC2 in host defense against both commensal and pathogenic bacteria.

Gut PGRP-SC2 functions as an antibacterial amidase

The sequence of PGRP-SC2 predicts a 20-amino-acid (aa) signal peptide at the N terminus, indicating that it functions as a secreted protein. To test it, we overexpressed a full-length PGRP-SC2 protein tagged with luciferase at the C terminus (PGRP-SC2-luci) in S2R^{+} cells. Compared with overexpression of a normal luciferase (luci) that stays inside the cells, the ratio of luciferase activities in the medium to cells was increased by >100-fold in S2R^{+} cells that express PGRP-SC2-luci fused proteins (Figure S1F), supporting that PGRP-SC2 is a secreted protein. PGRP-SC2 has been predicted to exhibit amidase activity to maintain gut-microbial homeostasis for decades (Royet and Dziarski, 2007); however, the biochemical evidence is still missing. We next examined the amidase activity of PGRP-SC2 by incubating synthetic PGNs together with mature PGRP-SC2 proteins (21-184aa) without signal peptide. SLP assays indicated that PGRP-SC2 decreased PGN amounts in a dose-dependent manner (Figure 4E), confirming its efficient amidase activity. The negative correlation between intestinal PGRP-SC2 expression and bacterial abundance suggested an antibacterial role of PGRP-SC2 (Figures 3D and 4C). To test this, we cultured different bacteria with mature PGRP-SC2 proteins and measured their growth using the alamar blue assays. We found that PGRP-SC2 significantly suppressed the growth of both Gram-negative (*Pseudomonas chlororaphis*, *Pseudomonas putida*, *Gluconobacter oxydans*, and *Acetobacteraceae gen.sp*) and Gram-positive (*Lactobacillus fermentum* and *Lactobacillus plantarum*) commensal bacteria in a dose-dependent manner (Figures 4F–4H). PGRP-SC2 also efficiently suppressed growth of multiple Gram-negative pathogenic bacteria (*Ecc15*, *Pseudomonas aeruginosa*, *Salmonella typhimurium*, and *Escherichia coli*) and some Gram-positive pathogenic bacteria (*Staphylococcus aureus*) at a higher concentration (Figures 4I and 4J). Therefore, we have identified PGRP-SC2 as an antibacterial amidase against both commensal and pathogenic bacteria.

Renal IMD-NF-κB blockade alleviates tumor-induced mortality

Previous studies have uncovered that IMD-NF-κB activation contributes to shortened lifespan (Garschall and Flatt, 2018). We then asked whether blockade of IMD-NF-κB signaling in yki^{3SA}-tumor-bearing flies is sufficient to improve mortality. To perform genetic manipulation in the context of yki^{3SA}-tumor growth, we integrated *LexA* and *GAL4* binary expression system, whereby we used *LexA* to induce yki^{3SA}-gut tumors and *GAL4* to manipulate gene expression in host organs. yki^{3SA}-tumor-bearing flies generated with *LexA* system exhibited similar but even severer systemic IMD-NF-κB activation and host wasting including lipid loss, hyperglycemia, muscle dysfunction, ovary atrophy, and shortened lifespan (Figures 5A–5C and S2). We next generated yki^{3SA}-gut tumors in *PGRP-LC^{E12}* or *Rel^{E20}* mutant flies to suppress systemic IMD-NF-κB signaling (Gottar et al., 2002; Hedengren et al., 1999). We found that both heterozygous and homozygous mutation of *PGRP-LC^{E12}* or *Rel^{E20}* potently suppressed IMD-NF-κB activation; however, only heterozygous *PGRP-LC^{E12}* and *Rel^{E20}* mutation significantly improved mortality without affecting yki^{3SA}-tumor growth or bloating or wasting phenotypes (Figures 5A–5D and S3A–S3B).

Please cite this article in press as: Chen et al., Renal NF-κB activation impairs uric acid homeostasis to promote tumor-associated mortality independent of wasting, Immunity (2022), https://doi.org/10.1016/j.immuni.2022.07.022

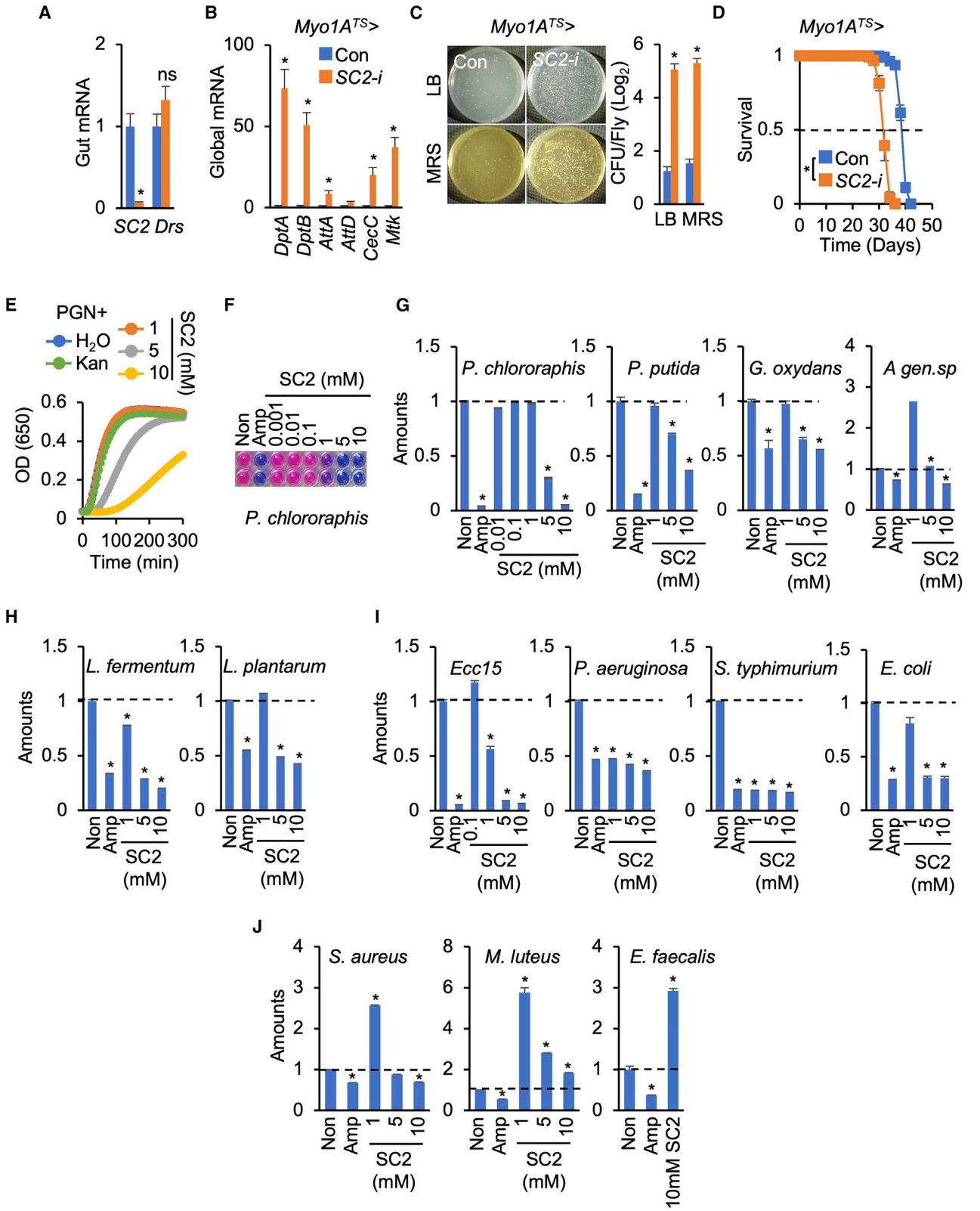

(legend on next page)

Please cite this article in press as: Chen et al., Renal NF-κB activation impairs uric acid homeostasis to promote tumor-associated mortality independent of wasting, Immunity (2022), https://doi.org/10.1016/j.immuni.2022.07.022

The homozygous *PGRP-LC*^{E12} mutation did not affect yki^{3SA}-tumor-induced mortality (Figure 5D), while the homozygous *Rel*^{E20} mutation even caused an early death with an exponential increase of gut bacteria (Figures S3C–S3E). These data suggest that IMD-NF-κB signaling contributes to yki^{3SA} tumors-induced mortality within a certain range probably due to tissue-specific roles regarding the balance between immune response and organ functions.

We next examined IMD-NF-κB activation in which tissues or organs contribute to yki^{3SA} tumors-induced mortality. As muscle and fat body have been established as the major contributing organs (Song et al., 2019), we silenced the expression of *Rel* in muscle or fat body using *Mhc*- or *R4-GAL4* in yki^{3SA} flies. However, *Rel* silencing in neither muscle nor fat body affected yki^{3SA}-tumor growth and its associated wasting effects or mortality (Figures 5E–5F and S4A–S4B and S4E). *Rel* silencing in the brain using *repo-GAL4* (Kounatidis et al., 2017) in yki^{3SA} flies also failed to affect energy wasting or mortality (Figures 5G and S4C and S4E), excluding the roles of IMD-NF-κB signaling in muscle, fat body, or brain in tumor-induced wasting or mortality.

We further examined other tissues and found that most of IMD-NF-κB target genes were potently induced in the renal-like Malpighian tubules (MTs) of yki^{3SA} flies compared with control ones (GSE204866) (Figure 5H and Table S2). *Rel* has been reported to be activated to induce gene transcription in the principal cells (PCs) of MTs in response to infection (Verma and Tapadia, 2012). Therefore, we used *c42-GAL4* to silence *Rel* expression and block IMD-NF-κB pathways in the renal PCs of yki^{3SA} flies. However, only *Rel*, but not *Tl*, silencing potently alleviated host death without affecting tumor growth or host wasting (Figures 5I–5J and S4D). Collectively, our results indicate that specific IMD-NF-κB activation in the renal organ potentiates mortality associated with yki^{3SA}-gut tumors.

Note that IMD-NF-κB signaling could be activated by, in addition to canonical PGN-PGRP-LC axis, STING that senses bacterial nucleotides and intestinal acetate that increases intracellular *PGRP-LC* transcription (Jugder et al., 2021; Martin et al., 2018). We investigated these possibilities of IMD-NF-κB activation as well. We analyzed the metabolomic changes in the hemolymph of yki^{3SA} flies (Kwon et al., 2015) but observed no induction in the acetate amounts in the hemolymph compared with controls (Table S3). We did not observe the induction of *PGRP-LC* transcription in the renal organ that is associated with acetate as well (Table S2). To assess the participation of STING pathway, we silenced *Sting* expression in the renal PCs of yki^{3SA} flies. However, we did not observe the suppression of IMD-NF-κB target gene expression in the renal organ or improvement of mortality (Figures S4F–S4G). These results suggest that bacterial acetate or nucleotides might not contribute to IMD-NF-κB activation in the renal PCs of yki^{3SA}-tumor-bearing flies.

Immune-associated UA accumulation promotes mortality of yki^{3SA}-tumor-bearing flies

We next investigated how renal IMD-NF-κB signaling affects survival of yki^{3SA}-tumor-bearing flies. It has been reported that the *Drosophila* renal organ potently regulates water and metabolite excretion, lipid transport, and urid acid metabolism, regarding animal survival (Lang et al., 2019; Li et al., 2020; van Dam et al., 2020). We analyzed the metabolomic changes in the hemolymph of yki^{3SA} flies compared with controls (Kwon et al., 2015) and observed that metabolites involved in purine metabolism were highly enriched (Figure 6A and Table S3). By analyzing each single metabolite of purine metabolism, we found that the ones associated with uric acid (UA) including guanine, hypoxanthine, xanthine, UA, allantoin, and allantoate were highly accumulated in the yki^{3SA} flies (Figures 6B and 6C). Single-cell RNA-seq analysis (Flycellatlas.org) (Li et al., 2022; Xu et al., 2022) uncovered that genes putatively involved in UA metabolism, including synthesis (*DhpD*, *Aox1*, *Aox3*, *ry*), transport (*Orct*, *CG6126*, *CG7881*, *MFS12*, *CG7882*, *w*, *st*, *Mrp4*, *CG4562*, *CG8654*), and catabolism (*Uro*, *CG30016*, *CG31763*, *Gip*) are predominantly expressed in renal PCs (Figures 6B and S5A–S5C). Further, expressional amounts of many genes involved in UA synthesis were increased, while those involved in UA excretion and catabolism were decreased, in the renal organ of yki^{3SA} flies (Figures 6B and 6D and S5D). We next examined the UA homeostasis in the renal organ of yki^{3SA} flies and observed large amounts of dark deposits suggestive of UA accumulation (Figure 6E). Consistently, we assayed UA content biochemically and found that excreted UA content was significantly decreased, while whole-body UA was increased, in yki^{3SA} flies (Figure 6F).

We next investigated the relationship between UA homeostasis, renal IMD-NF-κB signaling, and survival of yki^{3SA} flies. We observed that either antibiotic treatment or PGRP-SC2 overexpression, which were shown to suppress IMD-NF-κB signaling and improve survival, of yki^{3SA} flies potently diminished renal dark deposits and UA accumulation (Figures 6G and 6H). Importantly, specific *Rel* silencing to block IMD-NF-κB signaling in the renal PCs was sufficient to restore expression of certain genes involved in UA catabolism and transport, remove renal dark deposits, and decrease UA content in yki^{3SA} flies (Figures 6I–6J and S5D), confirming essential roles of renal IMD-NF-κB activation in tumor-associated UA accumulation. To examine whether UA overload promotes mortality of yki^{3SA} flies, we fed them allopurinol (AP), a small molecule efficiently preventing the conversion

Figure 4. PGRP-SC2 is a general antibacterial amidase

(A–C) qPCR analysis of gene expression in the midgut (A, n = 4, 10 flies/replicate) and whole body (B, n = 6, 5 flies/replicate) and bacterial loads (C, left, images of bacteria on agar plates; right, quantification, n = 4, 5 flies/replicate) in the gut of flies with or without *PGRP-SC2* RNAi in the ECs of control flies under normal feeding for 10 days.

(D) Lifespans of indicated flies (n = 100) (Log rank test, $p < 0.001$). (E) *In vitro* digestion of 1000 ng/μL PGN by H_2O, recombinant PGRP-SC2 proteins and antibiotic (Kan).

(F–I) Growth rates of different bacteria indicated by alamar blue under treatment of H_2O/PBS (Non), antibiotics (Amp/Kan), or recombinant PGRP-SC2 proteins in 96-well plates (F) and the fluorescent quantifications; (G–I, n = 3) (G, Gram-negative commensals; H, Gram-positive commensals; I, Gram-negative pathogens; J, Gram-positive pathogens).

Data are representative of at least three independent experiments. Data are presented as mean ± SEM Student's *t* test; *$p < 0.05$. "ns" indicates statistically non-significant. See also Figure S1.

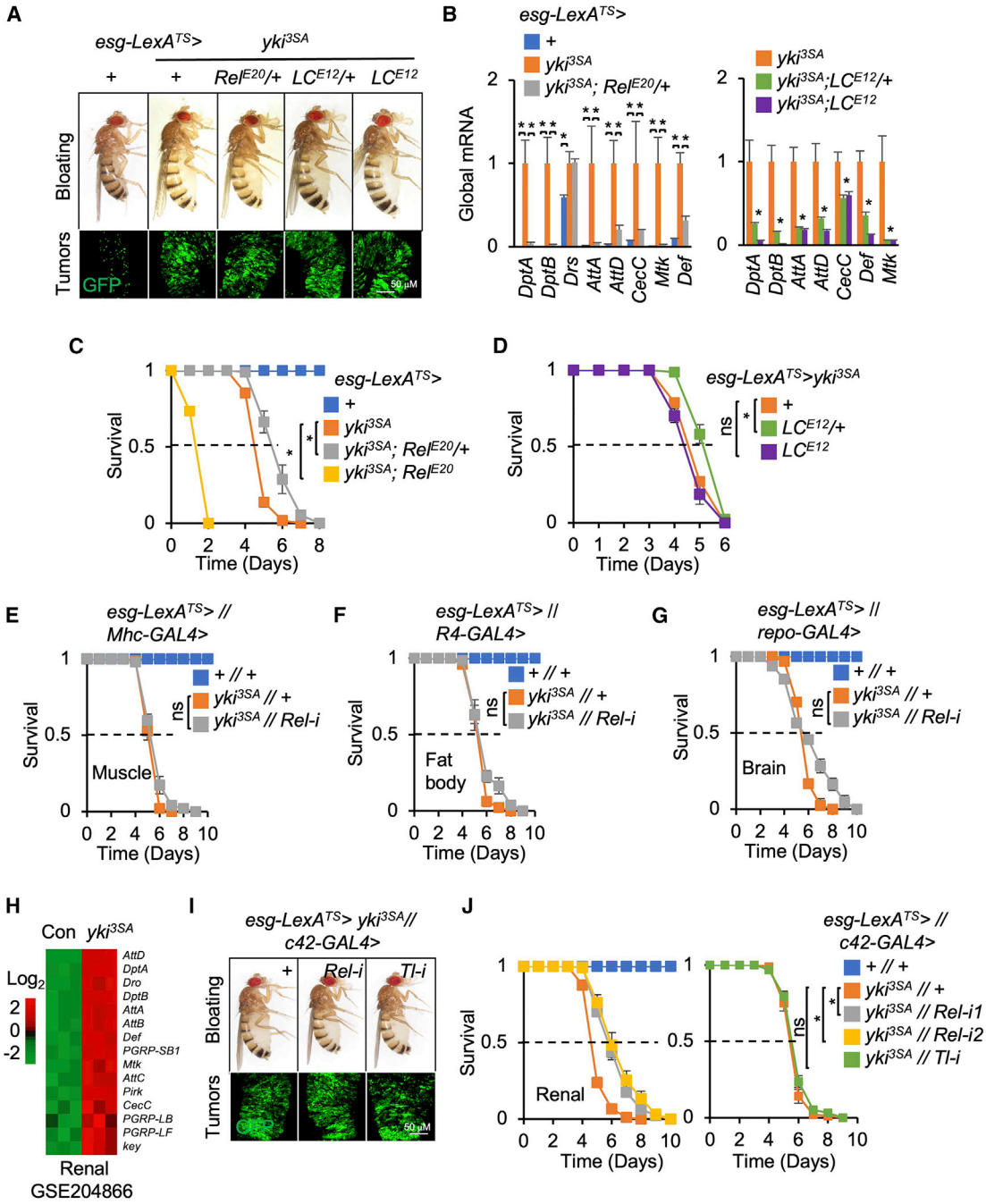

Figure 5. Renal blockade of IMD-NF-κB signaling improves yki^{3SA}-tumor-associated mortality

(A and B) Bloating and gut tumors (GFP) (A) and whole-body qPCR analysis (B, n = 6, 5 flies/replicate) of flies with mutation of *Rel* (*Rel^{E20}*) or *PGRP-LC* (*LC^{E12}*) under yki^{3SA}-tumor induction for 4 days using *LexA* system.

(C and D) Longevities of indicated flies (n = 100) (Log rank test, *yki^{3SA}* versus *yki^{3SA}; Rel^{E20}/+*, $p < 0.001$; *yki^{3SA}* versus *yki^{3SA}; Rel^{E20}*, $p < 0.001$; *yki^{3SA}* versus *yki^{3SA}; LC^{E12}/+*, $p < 0.001$).

(E–G) Longevities of flies under yki^{3SA}-tumor-induction using *LexA* system and tissue-specific *Rel* silencing using *GAL4* system (n = 120).

(H) Heatmap of RNA-seq data showing up-regulated target genes of IMD-NF-κB signaling in renal-like Malpighian tubules (MTs) of flies under yki^{3SA}-tumor induction for 8 days using *GAL4* system.

(I) Bloating and gut tumors (GFP) of flies under yki^{3SA}-tumor induction using *LexA* system and tissue-specific gene silencing using *GAL4* system for 4 days

(J) Longevities of indicated flies (n = 120) (Log rank test, *yki^{3SA}//+* versus *yki^{3SA}//Rel-i1*, $p < 0.001$; *yki^{3SA}//+* versus *yki^{3SA}//Rel-i2*, $p < 0.001$).

(B–G, and J) Data are representative of at least three independent experiments.

Data are presented as mean ± SEM Student's *t* test; *$p < 0.05$. "ns" indicates statistically non-significant. See also Figures S2–S4 and Tables S2 and S3.

Please cite this article in press as: Chen et al., Renal NF-κB activation impairs uric acid homeostasis to promote tumor-associated mortality independent of wasting, Immunity (2022), https://doi.org/10.1016/j.immuni.2022.07.022

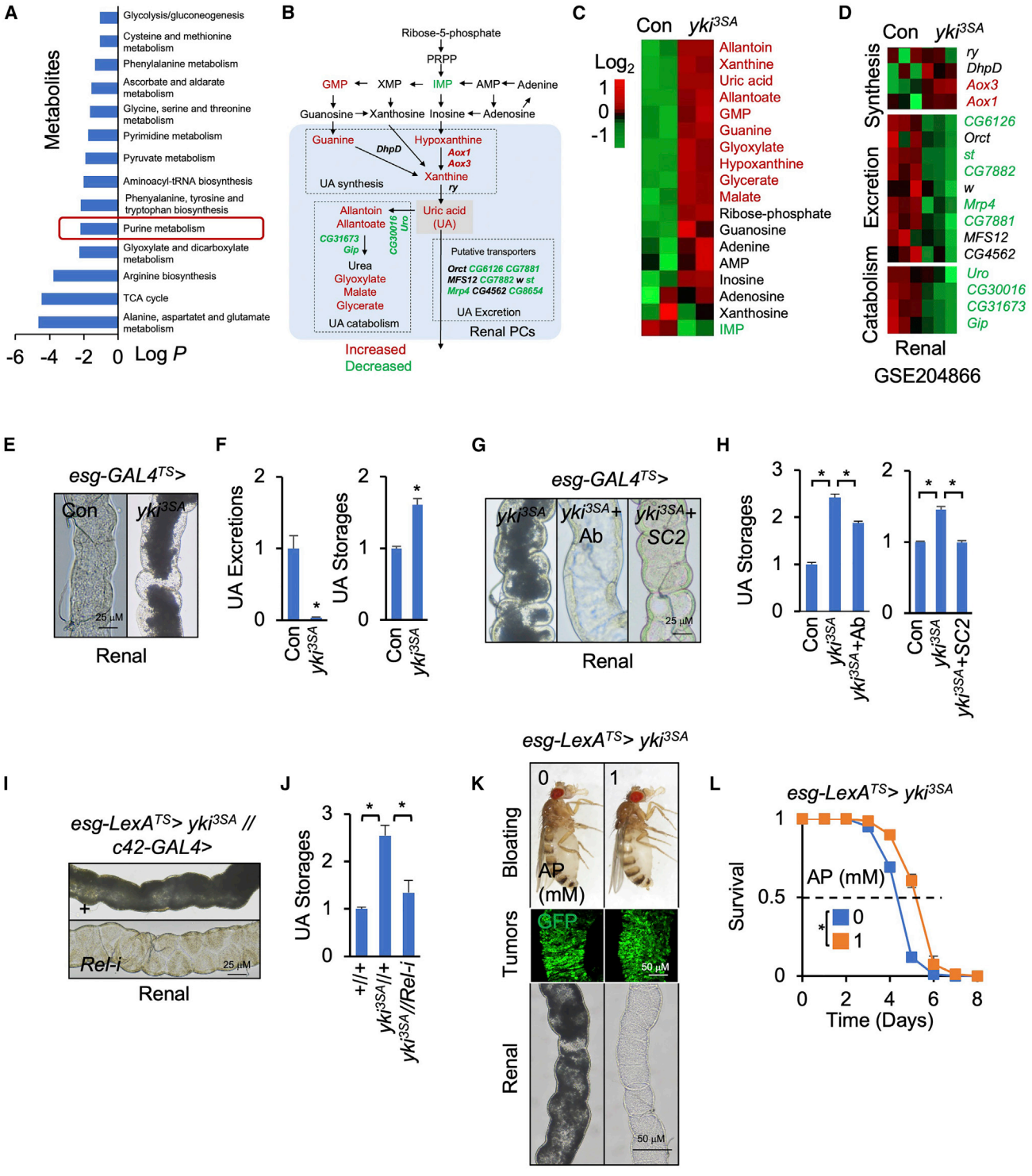

Figure 6. Rel-induced UA accumulation promotes mortality of yki^{3SA}-tumor-bearing flies

(A) Enrichment analysis of differentially changed metabolites in the hemolymph of flies under yki^{3SA}-tumor induction for 8 days using *GAL4* system.

(B) The schematic showing uric acid metabolism in *Drosophila*. Increased (red) and decreased (green) metabolites in the hemolymph or genes in the MTs of flies were indicated under yki^{3SA}-tumor induction for 8 days.

(C and D) Heatmap showing differentially changed hemolymph metabolites (C) and renal PC genes (D) in flies under yki^{3SA}-tumor induction for 8 days using *GAL4* system.

(legend continued on next page)

Please cite this article in press as: Chen et al., Renal NF-κB activation impairs uric acid homeostasis to promote tumor-associated mortality independent of wasting, Immunity (2022), https://doi.org/10.1016/j.immuni.2022.07.022

of xanthine to UA (Lang et al., 2019). Administration of 1 mM AP in the food potently diminished UA accumulation and improved the survival rates without affecting the tumor growth or bloating phenotypes of yki^{3SA} flies (Figures 6K and 6L), even though 1 mM AP was shown to potently shorten the lifespan of non-tumor control flies (data not shown) (Lang et al., 2019; van Dam et al., 2020). Taken together, our results demonstrate that renal IMD-NF-κB activation impairs UA homeostasis to promote mortality of yki^{3SA}-tumor-bearing flies.

Tumor-secreted proteins differentially regulate mortality via modulation of renal UA metabolism

Tumor-secreted proteins like ImpL2, Pvf1, and Upd3 are essential for wasting development of yki^{3SA}-tumor-bearing flies (Ding et al., 2021; Kwon et al., 2015; Song et al., 2019). We wondered whether they regulate survival of yki^{3SA}-tumor flies through the immune-UA axis. We silenced the expression of each of them in the gut tumors, which have been shown to alleviate wasting effects without affecting tumor growth. Removal of *ImpL2* in the gut tumors robustly abolished renal black deposits and systemic UA accumulation, leading to increased survival rates of yki^{3SA} flies (Figures 7A–7C). Because ImpL2 suppresses systemic insulin signaling and activates FoxO that has been shown to suppress *PGRP-SC2* transcription in the gut (Guo et al., 2014), we wondered whether the improvements in UA metabolism and mortality were associated with gut PGRP-SC2 production. We examined the gene expression in the gut and observed that tumor-induced *PGRP-SC2* suppression was only mildly restored, while induction of the FoxO-target gene *4EBP* was largely restored, by removal of tumor-derived ImpL2 (Figure 7D). Note that tumor-derived ImpL2 did not affect tumor-associated gut bacterial overload or systemic IMD-NF-κB activation (Figures 7E and 7F). To confirm these results, we further silenced *FoxO* expression specifically in ECs of yki^{3SA} guts and consistently found that *PGRP-SC2* expression was mildly restored compared with robust blunt of *4EBP* induction (Figure S6B). Again, EC *FoxO* deficiency failed to alleviate tumor growth, bloating phenotypes, systemic IMD-NF-κB activation, or UA accumulation in the renal organ (Figure S6A and 6C). These results suggest that ImpL2-FoxO axis participates in tumor-associated *PGRP-SC2* suppression only in a minor manner.

The observations suggest direct ImpL2 regulation of renal functions regarding high *InR* expression in PCs (Figure S5A; Soderberg et al., 2011). To address this issue, we increased insulin signaling in PCs by overexpressing an active Akt, myrAkt (DiAngelo et al., 2009). We found that Akt activation in the renal PCs potently increased renal UA metabolic gene expression, diminished renal UA accumulation, and improved mortality of yki^{3SA} flies without affecting tumor growth or bloating phenotypes (Figures 7G–7J). Note that Akt activation did not alleviate induction of Rel target gene expression in the PCs (Figure 7I), suggesting a Rel-independent role. Thus, our results reveal that tumor-derived ImpL2 results in renal UA accumulation and promotes mortality via modulation of insulin signaling and UA metabolism in the renal PCs in a manner independent of gut PGRP-SC2 and systemic IMD-NF-κB activation (Figure 7K).

We next investigated the effects of Upd3. Because we have shown the essential role of Upd3 in yki^{3SA}-tumor growth, we silenced *Upd3* expression in the yki^{3SA} + hop^{TumL} tumors that maintain intracellular Jak/Stat signaling and self-growth independent of extracellular Upd3 as we previously described (Ding et al., 2021). However, *Upd3* removal in the gut tumors failed to affect renal UA accumulation and mortality of tumor-bearing flies (Figures S6D–S6F).

Finally, we examined the roles of tumor-derived Pvf1. Similar to *ImpL2*, *Pvf1* removal in yki^{3SA} tumors potently abolished renal UA accumulation and increased survival rates of tumor-bearing flies (Figures S7A–S7C). However, tumor-*Pvf1* removal also potently alleviated bacterial overload and systemic IMD-NF-κB activation, regardless of no change in gut *PGRP-SC2* suppression (Figures S7D–S7F). Due to strong *Pvr* expression in the renal PCs (Figure S5A; Wang and Spradling, 2020), we also assessed Pvf1 impacts on the renal organ by overexpressing a dominant-negative Pvr, *Pvr^{DN}*, to block Pvr signaling in the PCs of yki^{3SA} flies. PC-Pvr overexpression unfortunately failed to alleviate tumor growth or bloating phenotypes, renal UA accumulation and IMD-NF-κB activation, and mortality (Figures S7G–S7J). Thus, our results indicate that tumor-derived Pvf1 triggers gut bacterial dysbiosis and systemic IMD-NF-κB activation through unclear mechanisms to result in UA accumulation and mortality.

DISCUSSION

Whether and how environmental factors and host immune response participate in wasting development and mortality regulation in tumor-bearing subjects is a missing piece in the cancer-cachexia field. Using *Drosophila* as a model organism to study gut bacteria that are mostly acquired from the environment, we establish that yki^{3SA}-gut-bearing tumors suppressed the production of antibacterial-amidase PGRP-SC2 and unleashed bacterial growth to activate IMD-NF-κB signaling specifically in the renal organ, leading to UA accumulation and mortality. Concomitantly, we also uncovered that tumor-secreted cachectic ImpL2 impacts renal UA metabolism and host death in an immune-independent manner.

PGRP-SC2 has been structurally predicted to have amidase activity to digest PGNs for decades (Royet et al., 2011); however, the biochemical evidence has not been available. In this study, we uncovered PGRP-SC2 as an antibacterial amidase due to its ability to degrade PGNs and generally suppress growth of

(E–J) Images indicating black deposits in the MTs (E, G, I) and whole body (F, H, J, n = 4, 5 flies/replicate) or excreted UA amounts (F, n = 4, 20 flies/replicate) of flies under yki^{3SA}-tumor induction for 8 days using *GAL4* system (E–H) or flies under yki^{3SA}-tumor induction for 4 days using *LexA* system and tissue-specific silencing of gene expression using *GAL4* system for 4 days (I–J).

(K) Abdomen bloating (left), gut tumors (middle, GFP), and MT black deposits (right) of flies under yki^{3SA}-tumor induction using *LexA* system with 1 mM AP feeding for 4 days.

(L) Longevities of indicated flies (n = 80) with 1 mM AP feeding throughout the lifespan (Log rank test, $p < 0.001$).

(F, H, J, and L) Data are representative of at least three independent experiments.

Data are presented as mean ± SEM Student's *t* test; *$p < 0.05$. "ns" indicates statistically non-significant. See also Figure S5 and Tables S2 and S3.

Please cite this article in press as: Chen et al., Renal NF-κB activation impairs uric acid homeostasis to promote tumor-associated mortality independent of wasting, Immunity (2022), https://doi.org/10.1016/j.immuni.2022.07.022

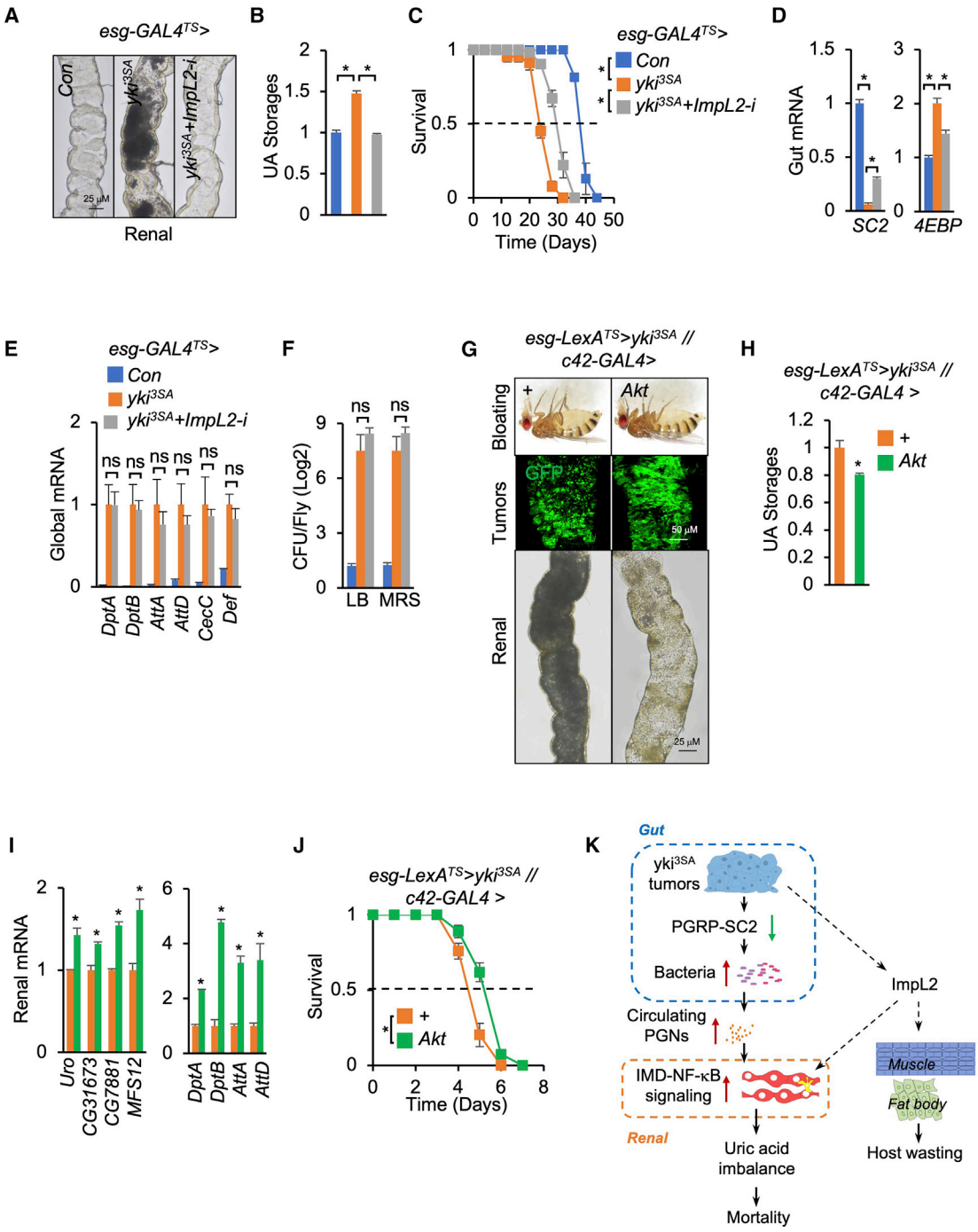

Figure 7. Tumor-derived ImpL2 promotes renal UA metabolism and host death via inhibition of insulin signaling in PCs

(A–F) Images showing MT black deposits (A), whole-body UA amounts (B, n = 4, 5 flies/replicate), midgut (D, n = 4, 10 flies/replicate), and whole-body (E, n = 6, 5 flies/replicate) gene expression indicated by qPCR, and quantification of gut bacterial loads (F, n = 4, 5 flies/replicate) of flies under induction of yki^{3SA} tumors with or without *ImpL2* silencing for 8 days using *GAL4* system.

(C) Longevities of indicated flies (n = 80) (Log rank test, *yki^{3SA}* versus *yki^{3SA}+ImpL2-i*, $p < 0.001$).

(G–I) Images showing abdomen bloating (left), gut tumors (middle, GFP), and black deposits in the renal (right) (G) whole-body UA amounts (H, n = 4, 5 flies/replicate), and renal gene expression indicated by qPCR (I, n = 4, 20 flies/replicate) of flies under yki^{3SA}-tumor induction for 4 days using *LexA* system and Akt overexpression in renal PCs for 4 days.

(J) Longevities of indicated flies (n = 80) (Log rank test, $p < 0.001$).

(K) The schematic model of regulation of mortality and host wasting by NF-κB-IMD signaling and tumor-secreted ImpL2 in yki^{3SA}-tumor-bearing flies.

(B–F and H–J) Data are representative of at least three independent experiments. Data are presented as mean ± SEM Student's *t* test; *$p < 0.05$. "ns" indicates statistically non-significant. See also Figures S6 and S7.

both commensal and pathogenic bacteria. Consistently, restoration of PGRP-SC2 expression in the gut of yki^{3SA} flies sufficiently alleviated, while *PGRP-SC2* deficiency in the ECs of control flies promoted, bacterial overload and systemic IMD-NF-κB activation and subsequent mortality. Further, EC *PGRP-SC2* deficiency potentiated *Ecc15*-induced IMD-NF-κB activation and mortality, confirming the general roles of PGRP-SC2 in restricting bacterial growth.

How yki^{3SA}-gut tumors affect PGRP-SC2 expression is another question to address. Because yki^{3SA}-gut-bearing tumors are generated from ISCs, while PGRP-SC2 is produced in ECs, we speculate an indirect regulation. We further found that both EC marker gene expression and EC composition were decreased in yki^{3SA}-tumor guts, indicating that yki^{3SA} induction in ISCs impairs general EC differentiation and decreases the mass of ECs that produce PGRP-SC2. On the other hand, we also examined the signaling pathways in the ECs, many of which have been reported to be perturbed by local tumors (Di Gregorio et al., 2016). Our results revealed that, at least, tumor-derived ImpL2-activated FoxO in the ECs slightly contributed to *PGRP-SC2* suppression; however, it did not sufficiently improve bacterial dysbiosis or systemic IMD-NF-κB activation of yki^{3SA} flies. Thus, we speculate that *PGRP-SC2* suppression is caused by both EC differentiation impairment and certain intracellular stress pathways that are worthy for investigation in our future studies.

In this study, we found that the mortality of yki^{3SA} flies was sufficiently improved by IMD-NF-κB blockade specifically in the renal organ, but not established energy-wasting tissues like muscle, fat body, or brain. Moreover, renal IMD-NF-κB blockade did not affect the host wasting features. These results collectively demonstrate that mortality of tumor-bearing subjects could be uncoupled from host energy wasting. Integrating metabonomics and tissue RNA-seq analysis, we uncovered that renal IMD-NF-κB activation resulted in host death via UA dysregulation. The mechanisms would include, at least, suppressing the expression of genes putatively involved in UA transport and catabolism in the renal PCs. Our results are consistent with previous studies of negative association between UA amounts and survival of normal flies (Lang et al., 2019; van Dam et al., 2020). Therefore, our findings of renal UA imbalance mediated by bacterial dysbiosis and NF-κB activation could be generally translated into mortality investigations in diverse disease models, including pathogen infection, aging, neurodegeneration, and high-caloric diets.

We have characterized three important tumor-secreted proteins (ImpL2, Pvf1, and Upd3) to cause host wasting. In this study, we further showed tumor-derived ImpL2 and Pvf1 promoted renal UA accumulation and host death in parallel with gut PGRP-SC2 production. For example, tumor-derived ImpL2 suppressed insulin-Akt signaling in PCs to impair UA metabolism. Meanwhile, Pvf1 promoted gut bacterial growth independent of PGRP-SC2 to activate systemic IMD-NF-κB signaling with unclear mechanisms. We speculate that Pvf1 might target fat body or muscle that has been shown to remotely modulate gut bacterial homeostasis (Chen et al., 2014; Zhao and Karpac, 2021). Even though Upd3 has been shown to disrupt the blood-brain barrier and cause fly death (Kim et al., 2021), we did not observe improvements in fly survival or renal UA accumulation by *Upd3* removal in gut tumors, suggesting the existence of other mechanisms.

Finally, our results are reminiscent of clinical observations of a negative correlation between circulating UA and general cancer survival (Shin et al., 2006; Strasak et al., 2007). It is reported that high serum UA (>6.7 mg/dL) is associated with increased risk of mortality of multiple cancers. However, the pathogenic regulation of hyperuricemia in advanced cancer patients is not well understood. Note that gut microbial dysbiosis has been extensively observed in patients and rodents bearing gastrointestinal and other tumors (Dutta and Lim, 2020; Vimal et al., 2020). Given the conserved regulation of gut commensal dysbiosis and its associated NF-κB activation in both *Drosophila* and mammals (Buchon et al., 2014; Peng et al., 2020), our findings of renal IMD-NF-κB modulating UA homeostasis provide uncharacterized mechanisms into hyperuricemia development and indicate targeting NF-κB-mediated gut-renal axis and UA maintenance as options for treatment and management of cancer-associated host death.

Limitations of the study

Several aspects of our model require further validation. First, even though we find that IMD-NF-κB signaling in renal organs, but not muscle, fat, or brain tissues, promotes mortality of yki^{3SA}-tumor-bearing flies, we have not excluded the impacts of other tissues like hepatocyte-like oenocytes, heart, and reproductive organs. Second, we have not provided the direct evidence of each IMD-NF-κB-associated gene that modulates renal UA catabolism and excretion. Third, bacterial elimination, renal IMD-NF-κB blockade, or UA depletion only partially, but not completely, restores survival of yki^{3SA}-tumor-bearing flies. Other potential mechanisms are still worthy to exploit in future studies.

STAR★METHODS

Detailed methods are provided in the online version of this paper and include the following:

- KEY RESOURCES TABLE
- RESOURCE AVAILABILITY
  - Lead contact
  - Materials availability
  - Data and code availability
- EXPERIMENTAL MODEL AND SUBJECT DETAILS
  - Fly strains and rearing
- METHOD DETAILS
  - Generation of transgenes
  - Generation of axenic flies
  - Infection of adults by *Ecc15*
  - Quantification of bacterial loads
  - Lipid and carbohydrate measurements in flies
  - Climbing activity
  - Electron microscopy
  - Uric acid measurement
  - Imaging of Malpighian tubule renal deposits
  - Gut staining and fly appearances imaging
  - Nanopore metagenome sequencing
  - RNA-seq analysis of adult Malpighian tubules

- qPCR analysis of gene expression
- Cell culture, constructs and luciferase assays
- Alamar blue cell viability assay
- Hemolymph PGN detection

- QUANTIFICATION AND STATISTICAL ANALYSIS

SUPPLEMENTAL INFORMATION

Supplemental information can be found online at https://doi.org/10.1016/j.immuni.2022.07.022.

ACKNOWLEDGMENTS

We thank the TsingHua Fly Center, TRiP at Harvard Medical School, Bloomington Drosophila Stock Center, and NIG in Japan for providing fly stocks; Lei Pan (Institute Pasteur of Shanghai) and Yingying Pu (Wuhan University) for bacteria strains; Heinrich Jasper (BUCK Institute) for *UAS-PGRP-SC2* flies; Pankaj Kapahi (BUCK Institute) for *c42-GAL4* flies; Zongzhao Zhai (Hunan Normal University) for Rel^{E20} and $PGRP\text{-}LC^{E12}$ flies; Yong Liu and Hong-bing Shu (Wuhan University) for comments and suggestions. Work in the Song lab was supported by the Chinese National Natural Science Foundation of China (91957118, 31800999, and 31971079), the Chinese Ministry of Science and Technology (National Key R&D Program, 2021YFC2700700), and the Fundamental Research Funds for the Central Universities, China.

AUTHOR CONTRIBUTIONS

Yuchen Chen designed and performed experiments, including molecular and metabolic assays, bacteria measurements, qPCR, genetic manipulation, and microbiota elimination. W.X. and Yuan Chen generated yki^{3SA}-tumor-bearing flies using *LexA* system. A.H. and J.S. helped perform bacterial assays and qPCR. X.Z. generated *UAS-PGRP-SC1* flies. W.S. and Yuchen Chen discussed results and wrote the manuscript.

DECLARATION OF INTERESTS

The authors declare no competing interests.

Received: December 28, 2021
Revised: May 27, 2022
Accepted: July 29, 2022
Published: August 26, 2022

REFERENCES

Ballarò, R., Costelli, P., and Penna, F. (2016). Animal models for cancer cachexia. Curr. Opin. Support. Palliat. Care *10*, 281–287. https://doi.org/10.1097/SPC.0000000000000233.

Baracos, V.E., Martin, L., Korc, M., Guttridge, D.C., and Fearon, K.C.H. (2018). Cancer-associated cachexia. Nat. Rev. Dis. Primers *4*, 17105. https://doi.org/10.1038/nrdp.2017.105.

Basset, A., Khush, R.S., Braun, A., Gardan, L., Boccard, F., Hoffmann, J.A., and Lemaitre, B. (2000). The phytopathogenic bacteria Erwinia carotovora infects Drosophila and activates an immune response. Proc. Natl. Acad. Sci. USA *97*, 3376–3381. https://doi.org/10.1073/pnas.97.7.3376.

Bischof, J., Maeda, R.K., Hediger, M., Karch, F., and Basler, K. (2007). An optimized transgenesis system for Drosophila using germ-line-specific phiC31 integrases. Proc. Natl. Acad. Sci. USA *104*, 3312–3317. https://doi.org/10.1073/pnas.0611511104.

Buchon, N., Silverman, N., and Cherry, S. (2014). Immunity in Drosophila melanogaster–from microbial recognition to whole-organism physiology. Nat. Rev. Immunol. *14*, 796–810. https://doi.org/10.1038/nri3763.

Capo, F., Wilson, A., and Di Cara, F. (2019). The Intestine of Drosophila melanogaster: An Emerging Versatile Model System to Study Intestinal Epithelial Homeostasis and Host-Microbial Interactions in Humans. Microorganisms *7*, E336. https://doi.org/10.3390/microorganisms7090336.

Charroux, B., and Royet, J. (2012). Gut-microbiota interactions in non-mammals: what can we learn from Drosophila? Semin. Immunol. *24*, 17–24. https://doi.org/10.1016/j.smim.2011.11.003.

Charroux, B., Capo, F., Kurz, C.L., Peslier, S., Chaduli, D., Viallat-Lieutaud, A., and Royet, J. (2018). Cytosolic and Secreted Peptidoglycan-Degrading Enzymes in Drosophila Respectively Control Local and Systemic Immune Responses to Microbiota. Cell Host Microbe *23*, 215–228.e4. https://doi.org/10.1016/j.chom.2017.12.007.

Chen, H., Zheng, X., and Zheng, Y. (2014). Age-associated loss of lamin-B leads to systemic inflammation and gut hyperplasia. Cell *159*, 829–843. https://doi.org/10.1016/j.cell.2014.10.028.

Costechareyre, D., Capo, F., Fabre, A., Chaduli, D., Kellenberger, C., Roussel, A., Charroux, B., and Royet, J. (2016). Tissue-Specific Regulation of Drosophila NF-kappaB Pathway Activation by Peptidoglycan Recognition Protein SC. J. Innate Immun. *8*, 67–80. https://doi.org/10.1159/000437368.

Di Gregorio, A., Bowling, S., and Rodriguez, T.A. (2016). Cell Competition and Its Role in the Regulation of Cell Fitness from Development to Cancer. Dev. Cell *38*, 621–634. https://doi.org/10.1016/j.devcel.2016.08.012.

DiAngelo, J.R., Bland, M.L., Bambina, S., Cherry, S., and Birnbaum, M.J. (2009). The immune response attenuates growth and nutrient storage in Drosophila by reducing insulin signaling. Proc. Natl. Acad. Sci. USA *106*, 20853–20858. https://doi.org/10.1073/pnas.0906749106.

Ding, G., Xiang, X., Hu, Y., Xiao, G., Chen, Y., Binari, R., Comjean, A., Li, J., Rushworth, E., Fu, Z., et al. (2021). Coordination of tumor growth and host wasting by tumor-derived Upd3. Cell Rep. *36*, 109553. https://doi.org/10.1016/j.celrep.2021.109553.

Dong, J., Yu, J., Li, Z., Gao, S., Wang, H., Yang, S., Wu, L., Lan, C., Zhao, T., Gao, C., et al. (2021). Serum insulin-like growth factor binding protein 2 levels as biomarker for pancreatic ductal adenocarcinoma-associated malnutrition and muscle wasting. J. Cachexia Sarcopenia Muscle *12*, 704–716. https://doi.org/10.1002/jcsm.12692.

Dutta, D., and Lim, S.H. (2020). Bidirectional interaction between intestinal microbiome and cancer: opportunities for therapeutic interventions. Biomark. Res. *8*, 31. https://doi.org/10.1186/s40364-020-00211-6.

Fearon, K., Arends, J., and Baracos, V. (2013). Understanding the mechanisms and treatment options in cancer cachexia. Nat. Rev. Clin. Oncol. *10*, 90–99. https://doi.org/10.1038/nrclinonc.2012.209.

Ferrandon, D., Imler, J.L., Hetru, C., and Hoffmann, J.A. (2007). The Drosophila systemic immune response: sensing and signalling during bacterial and fungal infections. Nat. Rev. Immunol. *7*, 862–874. https://doi.org/10.1038/nri2194.

Figueroa-Clarevega, A., and Bilder, D. (2015). Malignant Drosophila tumors interrupt insulin signaling to induce cachexia-like wasting. Dev. Cell *33*, 47–55. https://doi.org/10.1016/j.devcel.2015.03.001.

Garschall, K., and Flatt, T. (2018). The interplay between immunity and aging in Drosophila. F1000Res. *7*, 160. https://doi.org/10.12688/f1000research.13117.1.

Gottar, M., Gobert, V., Michel, T., Belvin, M., Duyk, G., Hoffmann, J.A., Ferrandon, D., and Royet, J. (2002). The Drosophila immune response against Gram-negative bacteria is mediated by a peptidoglycan recognition protein. Nature *416*, 640–644. https://doi.org/10.1038/nature734.

Guo, L., Karpac, J., Tran, S.L., and Jasper, H. (2014). PGRP-SC2 promotes gut immune homeostasis to limit commensal dysbiosis and extend lifespan. Cell *156*, 109–122. https://doi.org/10.1016/j.cell.2013.12.018.

Hedengren, M., Dushay, M.S., Dushay, M.S., Ando, I., Ekengren, S., Wihlborg, M., and Hultmark, D. (1999). Relish, a central factor in the control of humoral but not cellular immunity in Drosophila. Mol. Cell *4*, 827–837. https://doi.org/10.1016/s1097-2765(00)80392-5.

Jugder, B.E., Kamareddine, L., and Watnick, P.I. (2021). Microbiota-derived acetate activates intestinal innate immunity via the Tip60 histone acetyltransferase complex. Immunity *54*, 1683–1697.e3. https://doi.org/10.1016/j.immuni.2021.05.017.

Kandarian, S.C., Nosacka, R.L., Delitto, A.E., Judge, A.R., Judge, S.M., Ganey, J.D., Moreira, J.D., and Jackman, R.W. (2018). Tumour-derived leukaemia inhibitory factor is a major driver of cancer cachexia and morbidity

in C26 tumour-bearing mice. J. Cachexia Sarcopenia Muscle *9*, 1109–1120. https://doi.org/10.1002/jcsm.12346.

Kim, J., Chuang, H.C., Wolf, N.K., Nicolai, C.J., Raulet, D.H., Saijo, K., and Bilder, D. (2021). Tumor-induced disruption of the blood-brain barrier promotes host death. Dev. Cell *56*, 2712–2721.e4. https://doi.org/10.1016/j.devcel.2021.08.010.

Kounatidis, I., Chtarbanova, S., Cao, Y., Hayne, M., Jayanth, D., Ganetzky, B., and Ligoxygakis, P. (2017). NF-kappaB Immunity in the Brain Determines Fly Lifespan in Healthy Aging and Age-Related Neurodegeneration. Cell Rep. *19*, 836–848. https://doi.org/10.1016/j.celrep.2017.04.007.

Kröger, C., Dillon, S.C., Cameron, A.D.S., Papenfort, K., Sivasankaran, S.K., Hokamp, K., Chao, Y., Sittka, A., Hébrard, M., Händler, K., et al. (2012). The transcriptional landscape and small RNAs of Salmonella enterica serovar Typhimurium. Proc. Natl. Acad. Sci. USA *109*, E1277–E1286. https://doi.org/10.1073/pnas.1201061109.

Kwon, Y., Song, W., Droujinine, I.A., Hu, Y., Asara, J.M., and Perrimon, N. (2015). Systemic organ wasting induced by localized expression of the secreted insulin/IGF antagonist ImpL2. Dev. Cell *33*, 36–46. https://doi.org/10.1016/j.devcel.2015.02.012.

Lang, S., Hilsabeck, T.A., Wilson, K.A., Sharma, A., Bose, N., Brackman, D.J., Beck, J.N., Chen, L., Watson, M.A., Killilea, D.W., et al. (2019). A conserved role of the insulin-like signaling pathway in diet-dependent uric acid pathologies in Drosophila melanogaster. PLoS Genet. *15*, e1008318. https://doi.org/10.1371/journal.pgen.1008318.

Lee, W.J., and Brey, P.T. (2013). How microbiomes influence metazoan development: insights from history and Drosophila modeling of gut-microbe interactions. Annu. Rev. Cell Dev. Biol. *29*, 571–592. https://doi.org/10.1146/annurev-cellbio-101512-122333.

Lemaitre, B., and Hoffmann, J. (2007). The host defense of Drosophila melanogaster. Annu. Rev. Immunol. *25*, 697–743. https://doi.org/10.1146/annurev.immunol.25.022106.141615.

Li, H., Janssens, J., De Waegeneer, M., Kolluru, S.S., Davie, K., Gardeux, V., Saelens, W., David, F.P.A., Brbić, M., Spanier, K., et al. (2022). Fly Cell Atlas: A single-nucleus transcriptomic atlas of the adult fruit fly. Science *375*, eabk2432. https://doi.org/10.1126/science.abk2432.

Li, X., Rommelaere, S., Kondo, S., and Lemaitre, B. (2020). Renal Purge of Hemolymphatic Lipids Prevents the Accumulation of ROS-Induced Inflammatory Oxidized Lipids and Protects Drosophila from Tissue Damage. Immunity *52*, 374–387.e6. https://doi.org/10.1016/j.immuni.2020.01.008.

Martin, M., Hiroyasu, A., Guzman, R.M., Roberts, S.A., and Goodman, A.G. (2018). Analysis of Drosophila STING Reveals an Evolutionarily Conserved Antimicrobial Function. Cell Rep. *23*, 3537–3550.e6. https://doi.org/10.1016/j.celrep.2018.05.029.

Mellroth, P., Karlsson, J., and Steiner, H. (2003). A scavenger function for a Drosophila peptidoglycan recognition protein. J. Biol. Chem. *278*, 7059–7064. https://doi.org/10.1074/jbc.M208900200.

Molaei, M., Vandehoef, C., and Karpac, J. (2019). NF-kappaB Shapes Metabolic Adaptation by Attenuating Foxo-Mediated Lipolysis in Drosophila. Dev. Cell *49*, 802–810.e6. e806. https://doi.org/10.1016/j.devcel.2019.04.009.

Newton, H., Wang, Y.F., Camplese, L., Mokochinski, J.B., Kramer, H.B., Brown, A.E.X., Fets, L., and Hirabayashi, S. (2020). Systemic muscle wasting and coordinated tumour response drive tumourigenesis. Nat. Commun. *11*, 4653. https://doi.org/10.1038/s41467-020-18502-9.

Nie, Y., Yu, S., Li, Q., Nirala, N.K., Amcheslavsky, A., Edwards, Y.J.K., Shum, P.W., Jiang, Z., Wang, W., Zhang, B., et al. (2019). Oncogenic Pathways and Loss of the Rab11 GTPase Synergize To Alter Metabolism in Drosophila. Genetics *212*, 1227–1239. https://doi.org/10.1534/genetics.119.302137.

Paredes, J.C., Welchman, D.P., Poidevin, M., and Lemaitre, B. (2011). Negative regulation by amidase PGRPs shapes the Drosophila antibacterial response and protects the fly from innocuous infection. Immunity *35*, 770–779. https://doi.org/10.1016/j.immuni.2011.09.018.

Peng, C., Ouyang, Y., Lu, N., and Li, N. (2020). The NF-kappaB Signaling Pathway, the Microbiota, and Gastrointestinal Tumorigenesis: Recent Advances. Front. Immunol. *11*, 1387. https://doi.org/10.3389/fimmu.2020.01387.

Petkau, K., Ferguson, M., Guntermann, S., and Foley, E. (2017). Constitutive Immune Activity Promotes Tumorigenesis in Drosophila Intestinal Progenitor Cells. Cell Rep. *20*, 1784–1793. https://doi.org/10.1016/j.celrep.2017.07.078.

Qiu, Y., Yu, S., Wang, Y., Xiao, L., Pei, L., Pu, Y., and Zhang, Y. (2022). Photothermal therapy may be a double-edged sword by inducing the formation of bacterial antibiotic tolerance. Biomater. Sci. *10*, 1995–2005. https://doi.org/10.1039/d1bm01740c.

Royet, J., and Dziarski, R. (2007). Peptidoglycan recognition proteins: pleiotropic sensors and effectors of antimicrobial defences. Nat. Rev. Microbiol. *5*, 264–277. https://doi.org/10.1038/nrmicro1620.

Royet, J., Gupta, D., and Dziarski, R. (2011). Peptidoglycan recognition proteins: modulators of the microbiome and inflammation. Nat. Rev. Immunol. *11*, 837–851. https://doi.org/10.1038/nri3089.

Ryu, J.H., Kim, S.H., Lee, H.Y., Bai, J.Y., Nam, Y.D., Bae, J.W., Lee, D.G., Shin, S.C., Ha, E.M., and Lee, W.J. (2008). Innate immune homeostasis by the homeobox gene caudal and commensal-gut mutualism in Drosophila. Science *319*, 777–782. https://doi.org/10.1126/science.1149357.

Shin, H.S., Lee, H.R., Lee, D.C., Shim, J.Y., Cho, K.H., and Suh, S.Y. (2006). Uric acid as a prognostic factor for survival time: a prospective cohort study of terminally ill cancer patients. J. Pain Symptom Manage. *31*, 493–501. https://doi.org/10.1016/j.jpainsymman.2005.11.014.

Söderberg, J.A.E., Birse, R.T., and Nässel, D.R. (2011). Insulin production and signaling in renal tubules of Drosophila is under control of tachykinin-related peptide and regulates stress resistance. PLoS One *6*, e19866. https://doi.org/10.1371/journal.pone.0019866.

Song, W., Kir, S., Hong, S., Hu, Y., Wang, X., Binari, R., Tang, H.W., Chung, V., Banks, A.S., Spiegelman, B., and Perrimon, N. (2019). Tumor-Derived Ligands Trigger Tumor Growth and Host Wasting via Differential MEK Activation. Dev. Cell *48*, 277–286.e6. e276. https://doi.org/10.1016/j.devcel.2018.12.003.

Strasak, A.M., Rapp, K., Hilbe, W., Oberaigner, W., Ruttmann, E., Concin, H., Diem, G., Pfeiffer, K.P., Ulmer, H.; VHM&PP Study Group, and Group, P.P.S. (2007). Serum uric acid and risk of cancer mortality in a large prospective male cohort. Cancer Causes Control. *18*, 1021–1029. https://doi.org/10.1007/s10552-007-9043-3.

Tisdale, M.J. (2002). Cachexia in cancer patients. Nat. Rev. Cancer *2*, 862–871. https://doi.org/10.1038/nrc927.

Toda, H., Williams, J.A., Gulledge, M., and Sehgal, A. (2019). A sleep-inducing gene, nemuri, links sleep and immune function in Drosophila. Science *363*, 509–515. https://doi.org/10.1126/science.aat1650.

Troha, K., Nagy, P., Pivovar, A., Lazzaro, B.P., Hartley, P.S., and Buchon, N. (2019). Nephrocytes Remove Microbiota-Derived Peptidoglycan from Systemic Circulation to Maintain Immune Homeostasis. Immunity *51*, 625–637.e3. https://doi.org/10.1016/j.immuni.2019.08.020.

van Dam, E., van Leeuwen, L.A.G., Dos Santos, E., James, J., Best, L., Lennicke, C., Vincent, A.J., Marinos, G., Foley, A., Buricova, M., et al. (2020). Sugar-Induced Obesity and Insulin Resistance Are Uncoupled from Shortened Survival in Drosophila. Cell Metab. *31*, 710–725.e7. https://doi.org/10.1016/j.cmet.2020.02.016.

Verma, P., and Tapadia, M.G. (2012). Immune response and anti-microbial peptides expression in Malpighian tubules of Drosophila melanogaster is under developmental regulation. PLoS One *7*, e40714. https://doi.org/10.1371/journal.pone.0040714.

Vimal, J., Himal, I., and Kannan, S. (2020). Role of microbial dysbiosis in carcinogenesis & cancer therapies. Indian J. Med. Res. *152*, 553–561. https://doi.org/10.4103/ijmr.IJMR_1026_18.

Wang, C., and Spradling, A.C. (2020). An abundant quiescent stem cell population in Drosophila Malpighian tubules protects principal cells from kidney stones. Elife *9*, e54096. https://doi.org/10.7554/eLife.54096.

Wang, L., Liu, Q., Chen, Y., Zheng, X., Wang, C., Qi, Y., Dong, Y., Xiao, Y., Chen, C., Chen, T., et al. (2022). Antioxidant potential of Pediococcus pentosaceus strains from the sow milk bacterial collection in weaned piglets. Microbiome *10*, 83. https://doi.org/10.1186/s40168-022-01278-z.

Xu, J., Liu, Y., Li, H., Tarashansky, A.J., Kalicki, C.H., Hung, R.J., Hu, Y., Comjean, A., Kolluru, S.S., Wang, B., et al. (2022). Transcriptional and functional motifs defining renal function revealed by single-nucleus RNA sequencing. Proc. Natl. Acad. Sci. USA *119*. e2203179119. https://doi.org/10.1073/pnas.2203179119.

Yeom, E., Shin, H., Yoo, W., Jun, E., Kim, S., Hong, S.H., Kwon, D.W., Ryu, T.H., Suh, J.M., Kim, S.C., et al. (2021). Tumour-derived Dilp8/INSL3 induces cancer anorexia by regulating feeding neuropeptides via Lgr3/8 in the brain. Nat. Cell Biol. *23*, 172–183. https://doi.org/10.1038/s41556-020-00628-z.

Zaidman-Rémy, A., Hervé, M., Poidevin, M., Pili-Floury, S., Kim, M.S., Blanot, D., Oh, B.H., Ueda, R., Mengin-Lecreulx, D., and Lemaitre, B. (2006). The Drosophila amidase PGRP-LB modulates the immune response to bacterial infection. Immunity *24*, 463–473. https://doi.org/10.1016/j.immuni.2006.02.012.

Zhai, Z., Boquete, J.P., and Lemaitre, B. (2018). Cell-Specific Imd-NF-kappaB Responses Enable Simultaneous Antibacterial Immunity and Intestinal Epithelial Cell Shedding upon Bacterial Infection. Immunity *48*, 897–910.e7. e897. https://doi.org/10.1016/j.immuni.2018.04.010.

Zhao, X., and Karpac, J. (2021). Glutamate metabolism directs energetic trade-offs to shape host-pathogen susceptibility in Drosophila. Cell Metab. *33*, 2428–2444.e8. e2428. https://doi.org/10.1016/j.cmet.2021.10.003.

Zhou, J., and Boutros, M. (2020). JNK-dependent intestinal barrier failure disrupts host–microbe homeostasis during tumorigenesis. Proc. Natl. Acad. Sci. USA *117*, 9401–9412. https://doi.org/10.1073/pnas.1913976117.

Please cite this article in press as: Chen et al., Renal NF-κB activation impairs uric acid homeostasis to promote tumor-associated mortality independent of wasting, Immunity (2022), https://doi.org/10.1016/j.immuni.2022.07.022

STAR★METHODS

KEY RESOURCES TABLE

REAGENT or RESOURCE	SOURCE	IDENTIFIER
Bacterial strains		
Escherichia coli (*E. coli*)	Vazyme	Cat#C502
Erwinia carotovora carotovora15 (*Ecc15*)	(Basset et al., 2000)	N/A
Enterococcus faecalis (*E. faecalis*)	(Wang et al., 2022)	N/A
Salmonella typhimurium (*S. typhimurium*)	(Kroger et al., 2012)	N/A
Micrococcus luteus (*M. luteus*)	CGMCC	Cat#1.9051
Staphylococcus aureus (*S. aureus*)	(Qiu et al., 2022)	N/A
Pseudomonas aeruginosa (*P. aeruginosa*)	CCTCC	Cat#AB2010174
Pseudomonas putida (*P. putida*)	CCTCC	Cat#AB2014017
Pseudomonas chlororaphis (*P. chlororaphis*)	CCTCC	Cat#AB200053
Gluconobacter oxydans (*G. oxydans*)	CCTCC	Cat#AB204035
Acetobacteraceae *gen. sp* (*A gen. sp*)	CCTCC	Cat#AB2012042T
Lactobacillus fermentum (*L. fermentum*)	CCTCC	Cat#AB2015067
Lactobacillus plantarum (*L. plantarum*)	CCTCC	Cat#AB2015024
Chemicals, peptides, and recombinant proteins		
Bradford reagent	Vazyme	Cat#E211-01
Amyloglucosidase	Sigma	Cat#A7420
Triglyceride reagent	Sigma	Cat#T2449-10ML
Free glycerol reagent	Sigma	Cat#F6428-40ML
Glycerol standard	Sigma	Cat#G7793-5ML
Trehalase	Megazyme	Cat#E-TREH
Glucose assay reagent	Megazyme	Cat#K-Gluc
D-(+)-Glucose	Sangon Biotech	Cat#A501991
HiScript II Q RT Supermix	Vazyme	Cat#R222-01
SYBR qPCR Master Mix	Vazyme	Cat#Q311-03
Trizol	Thermo Fisher Scientific	Cat#15596018
DAPI	Thermo Fisher Scientific	Cat#D1306
Alamar blue	Thermo Fisher Scientific	Cat#DL1025
Vectashield	Vector	Cat#H-1000
Allopurinol	TargetMol	Cat#T0692
Carbenicillin, disodium salt	Sangon Biotech	Cat#A100358
Metronidazole	Sangon Biotech	Cat#A600633
Tetracycline hydrochloride	Sangon Biotech	Cat#A100422
Ampicillin sodium	Sangon Biotech	Cat#A610028
Kanamycin sulfate	Sangon Biotech	Cat#A600286
Critical commercial assays		
Triglyceride Assay Kit	Sigma	Cat#T2449
Trehalose Assay Kit	Megazyme	Cat#K-Gluc
Effectene Transfection Reagent	QIAGEN	Cat#301425
Uric Acid Assay Kit	BioAssay Systems	Cat#DIUA-250
ClonExpress MultiS One Step Cloning Kit	Vazyme	Cat#C113-01
Dual-Luciferase Reporter assay kit	Promega	Cat#E1910
SLP Reagent Kit	Fujifilm Wako Pure Chemical Corporation	Cat#297-51501
Fecal DNA extacting kit	Tiangen	Cat#DP328

(*Continued on next page*)

Please cite this article in press as: Chen et al., Renal NF-κB activation impairs uric acid homeostasis to promote tumor-associated mortality independent of wasting, Immunity (2022), https://doi.org/10.1016/j.immuni.2022.07.022

Continued

REAGENT or RESOURCE	SOURCE	IDENTIFIER
Deposited data		
Metagenomic data from fly guts	This study	GEO: GSE204975
RNA-seq data from fly Malpighian tubules	This study	GEO: GSE204866
RNA-seq data from fly midgut	(Song et al., 2019)	GEO: GSE113728
RNA-seq data from fly muscle	(Kwon et al., 2015)	GEO: GSE65325
Experimental models: Cell lines		
D. melanogaster: Cell line S2R^{+}	Laboratory of Norbert Perrimon, Harvard Medical School	N/A
Experimental models: Organisms/strains		
Drosophila melanogaster: *esg-GAL4*, *tub-GAL80^{TS}*, *UAS-GFP*	(Song et al., 2019)	N/A
Drosophila melanogaster: *Myo1A-GAL4*, *esg-GFP*; *tub-GAL80^{TS}*	(Song et al., 2019)	N/A
Drosophila melanogaster: *R4-GAL4*	(Song et al., 2019)	N/A
Drosophila melanogaster: *Mhc-GAL4*	(Song et al., 2019)	N/A
Drosophila melanogaster: *w^{1118}*	(Song et al., 2019)	N/A
Drosophila melanogaster: *UAS-hop^{TumL}*	(Song et al., 2019)	N/A
Drosophila melanogaster: *UAS-PGRP-SC2*	Dr. Heinrich Jasper, BUCK Institute (Guo et al., 2014)	N/A
Drosophila melanogaster: *c42-GAL4*	Dr. Pankaj Kapahi, BUCK Institute (Lang et al., 2019)	N/A
Drosophila melanogaster: *Repo-GAL4*	Center for Excellence in Molecular Cell Science, Chinese Academy of Sciences	N/A
Drosophila melanogaster: *Rel^{E20}*	Dr. Zongzhao Zhai, Hunan Normal University, China (Zhai et al., 2018)	N/A
Drosophila melanogaster: *PGRP-LC^{E12}*	Dr. Zongzhao Zhai, Hunan Normal University, China (Zhai et al., 2018)	N/A
Drosophila melanogaster: *UAS-Rel-RNAi*	Bloomington Stock Center	BDSC_33661
Drosophila melanogaster: *UAS-Rel-RNAi*	Bloomington Stock Center	BDSC_28943
Drosophila melanogaster: *UAS-Sting-RNAi*	Bloomington Stock Center	BDSC_31565
Drosophila melanogaster: *UAS-FoxO-RNAi*	Bloomington Stock Center	BDSC_27656
Drosophila melanogaster: *UAS-Tl-RNAi*	Bloomington Stock Center	BDSC_31477
Drosophila melanogaster: *UAS-Upd3-RNAi*	Bloomington Stock Center	BDSC_28575
Drosophila melanogaster: *esg-LexA.RJ-4*	Bloomington Stock Center	BDSC_66630
Drosophila melanogaster: *LexAop-GFP*	Bloomington Stock Center	BDSC_32205
Drosophila melanogaster: *LexAop-cdTomato*	Bloomington Stock Center	BDSC_77139
Drosophila melanogaster: *UAS-yki^{3SA}*	Bloomington Stock Center	BDSC_28817
Drosophila melanogaster: *UAS-Pvr^{DN}*	Bloomington Stock Center	BDSC_58431
Drosophila melanogaster: *UAS-myr-Akt*	Bloomington Stock Center	BDSC_80935
Drosophila melanogaster: *UAS-ImpL2-RNAi*	Bloomington Stock Center	BDSC_64936
Drosophila melanogaster: *UAS-PGRP-SC2-RNAi*	National Institute of Genetics	NIG_14745R-1
Drosophila melanogaster: *UAS-Pvf1-RNAi*	National Institute of Genetics	NIG_7103R-1
Drosophila melanogaster: *UAS-PGRP-SC1*	This study	N/A
Drosophila melanogaster: *LexAop-yki^{3SA} (attP40)*	This study	N/A
Drosophila melanogaster: *LexAop-yki^{3SA} (attP2)*	This study	N/A
Oligonucleotides		
Primer for cloning of *yki^{3SA}*, forward: CCGCTCGAGATGTGCGCGTGCCTAATCGC	This study	N/A
Primer for cloning of *yki^{3SA}*, reverse: GCTCTAGATTACGTAGAATCGAGA CCGAGGAGAGGG	This study	N/A

(*Continued on next page*)

Please cite this article in press as: Chen et al., Renal NF-κB activation impairs uric acid homeostasis to promote tumor-associated mortality independent of wasting, Immunity (2022), https://doi.org/10.1016/j.immuni.2022.07.022

Continued

REAGENT or RESOURCE	SOURCE	IDENTIFIER
Primer for cloning of *PGRP-SC1*, forward: TAGTCCAGTGTGGTGGAATTCATGGTTT CCAAAGTGGCTC	This study	N/A
Primer for cloning of *PGRP-SC1*, reverse: GCTCTAGATTACGTAGAATCGAGACCG AGGAGAGGG	This study	N/A
Primer for cloning of *PGRP-SC2*, forward: ACTAGTCCAGTGTGGTGGATGGCAAAC AAAGCTCTC	This study	N/A
Primer for cloning of *PGRP-SC2*, reverse: GTTTTTGGCGTCTTCCATGGCCTTCCA GTTGGACCAG	This study	N/A
Primer for cloning of *Luciferase*, forward: TACTAGTCCAGTGTGGTGGAATTCATG GAAGACGCCAAAAACATAAAG	This study	N/A
Primer for cloning of *Luciferase*, reverse: CTGTGCTGGATATCTGCAGAATTCTTAC ACGGCGATCTTTCCGCCCTTCTT	This study	N/A
Primers for qPCR, see Table S4	This study	N/A
Recombinant DNA		
pJFRC19-13XLexAop2-IVS-myr::GFP	Addgene	Cat#26224
pUAST-attB	(Bischof et al., 2007)	N/A
pUAST-attB-PGRP-SC1	This study	N/A
pGL3-Basic	Promega	Cat#E1751
pAc5.1	Thermo Fisher Scientific	Cat#V411020
pAc5.1-Luci	This study	N/A
pAc5.1-PGRP-SC2-Luci	This study	N/A
Software and algorithms		
Prism 8	GraphPad	https://www.graphpad.com/scientific-software/prism/
ImageJ	ImageJ	https://ImageJ.nih.gov/ij/
Adobe Photoshop CS6	Adobe	https://www.adobe.com/
R (v4.0.4)	R Core Team	https://www.r-project.org/

RESOURCE AVAILABILITY

Lead contact

Further information and requests for resources and reagents should be directed to and will be fulfilled by the lead contact, Wei Song (songw@whu.edu.cn).

Materials availability

All stable reagents generated in this study are available from the lead contact without restriction.

Data and code availability

This paper analyzes existing, publicly available data. These accession numbers for the datasets are listed in the key resources table. This paper does not report original code. Any additional information required to reanalyze the data reported in this paper is available from the lead contact upon request.

EXPERIMENTAL MODEL AND SUBJECT DETAILS

Fly strains and rearing

All flies were grown on the food containing 5.5 g agar, 65 g sucrose, 25 g dry yeast, 65 g cornmeal, 4 mL propionic acid, and 1.25 g Methylparaben (dissolved in 95% ethanol) per liter under standard laboratory conditions (25 °C, 12:12 h light/dark).

Please cite this article in press as: Chen et al., Renal NF-κB activation impairs uric acid homeostasis to promote tumor-associated mortality independent of wasting, Immunity (2022), https://doi.org/10.1016/j.immuni.2022.07.022

To induce gut tumors, we followed the experimental procedures described previously (Song et al., 2019). Briefly, different *UAS* and *LexAop* insertions were crossed to *esg-GAL4*, *tub-GAL80^{TS}*, *UAS-GFP* and *esg-LexA*, *tub-GAL80^{TS}*, *LexAop-GFP* at 18 °C, respectively, to inactivate *GAL4* and *LexA*. 4-day-old female adult progenies were placed at 29 °C to induce the transgenes (day 0 for tumor induction). During incubation at 29 °C, flies were transferred onto fresh food every 2 days. For antibiotic (Ab) treatment, standard medium was supplemented with 150 μg/mL carbenicillin, 150 μg/mL metronidazole, and 75 μg/mL tetracyclin. For drug treatment, the standard medium was supplemented with 1 mM allopurinol (TargetMol, UAS. T0692).

To silence gene expression in adult ECs, we crossed *UAS-RNAi* to *Myo1A-GAL4*, *esg-GFP*; *tub-GAL80^{TS}* at 18 °C. 4-day-old female adult progenies were placed at 29 °C to induce RNAi (day 0 for RNAi induction). During incubation at 29 °C, flies were transferred onto fresh food every 2 days.

For lifespan measurements, adults were cultured at 29 °C and transferred onto fresh food with or without antibiotics or allopurinol every 2 days for *GAL4-UAS* system or every day for *LexA-LexAop* system. All experiments were performed at least 3 times.

METHOD DETAILS

Generation of transgenes

To generate *LexAop-yki^{3SA}* flies, we amplified *yki^{3SA}* fragment using the primers: forward: CCGCTCGAGAT-GTGCGCGTGCC TAATCGC and reverse: GCTCTAGATTACGTAGAATCGAGACCGAGGAGAGGG. The PCR product was cloned into 13XLexAop2-IVS-myr:GFP vector (Addgene, 26,224) at the *XhoI* and *XbaI* sites. The 13XLexAop-yki^{3SA} construct was targeted into the attP2 or attP40 site through standard germline transformation.

To generate *UAS-PGRP-SC1* flies, the following primers, forward: TAGTCCAGTGTGGTGGAATTC-ATGGTTTCCAAAGTGGCTC and reverse: GCTCTAGATTACGTAGAATCGAGACCGAGGAGAGGG, were used to amplify PGRP-SC1 fragment. The PCR product was cloned into pUAST-attB vector (Bischof et al., 2007) at *EcoRI* and *EcoRV* sites and targeted into the attP2 site through standard germline transformation.

Generation of axenic flies

To generate germ-free flies, 0-6h embryos were collected on grape juice plates, washed with sterile water and then bleached with 3% solution of sodium hypochlorite for 3 min. Embryos were subsequently washed twice in 70% ethanol, followed by two washes with sterile water. The embryos were then maintained with axenic food and routinely checked for bacterial contamination by culturing the food and homogenate on LB and MRS agar plates.

Infection of adults by *Ecc15*

The monoclonal bacteria *Ecc15* were cultured overnight by shaking at 200 rpm at 30 °C. Bacterial were collected after centrifuging at 6,000 x *g* for 10 min at 4 °C and washed twice with sterile PBS at 7,500 x *g* for 5 min at 4 °C. The bacteria were resuspended with sterile 5% sucrose solution as OD_{600} = 200. For oral infection, 4–6 days female flies were starved for 2h prior to being transferred in vials fully covered by two layers of filter paper containing 200 μL *Ecc15*. Adult flies were transferred to vials with fresh *Ecc15* every 2 days.

Quantification of bacterial loads

The outside surface of flies was rinsed with 70% ethanol for 1 to 2 min, and washed twice with sterile water. 5 flies were individually homogenized in 200 μL sterile PBS using multi-sample tissuelyser-24 (Shanghai Jingxin Technology). 50 μL homogenate were plated onto LB and MRS agar plates by using Glass Beads (Sangon Biotech, B529319) and were incubated at 29 °C for 2 days prior to counting colony forming unit (CFU). All experiments were performed at least 3 times.

Lipid and carbohydrate measurements in flies

We measured fly TAG and carbohydrates as described previously (Song et al., 2019). Briefly, 5 flies from each group were homogenized with 500 μL PBS containing 0.2% Triton X-100 using multi-sample tissuelyser-24 (Shanghai Jingxin Technology) and heated at 70 °C for 5 min. The supernatant was collected after centrifugation at 12,000 x *g* for 15 min at 4 °C. 10 μL of supernatant was used for protein quantification using Bradford Reagent (Vazyme, E211-01). Whole body trehalose and glycogen amounts were measured from 10 μL of supernatant treated with 0.2 μL trehalase (Megazyme, E-TREH) and 0.8 μL Amyloglucosidase (Sigma, A7420), respectively, at 37 °C for 20 min using glucose assay reagent (Megazyme, K-GLUC) following the manufacturer's protocol. We subtracted the amounts of free glucose from the measurement and then normalized to protein amounts in the supernatant. To measure whole body triglyceride amounts, we processed 10 μL of supernatant using a Serum Triglyceride Determination kit (Sigma, TR0100), subtracted the amounts of free glycerol in the supernatant from the measurement, and then normalized to protein amounts in the supernatant.

Climbing activity

Flies were placed in an empty vial and then tapped down to the bottom. They were allowed to climb for 3 s. Climbing was filmed and climbing height and speed were calculated from the video using ImageJ. A minimum of 15 flies and 10 separate trials were performed for each condition.

Please cite this article in press as: Chen et al., Renal NF-κB activation impairs uric acid homeostasis to promote tumor-associated mortality independent of wasting, Immunity (2022), https://doi.org/10.1016/j.immuni.2022.07.022

Electron microscopy

Adult thoraces were processed and analyzed in cross-section following protocols as described previously (Ding et al., 2021). Briefly, thoraces were fixed in 0.1 M sodium cacodylate buffer (pH 7.4) containing 2.5% glutaraldehyde, 2% paraformaldehyde overnight. The fixed samples were washed in 0.1 M cacodylate buffer, fixed again with 1% osmium tetroxide (OsO4) and 1.5% potassium ferrocyanide (KFeCN6) for 1 h, and washed 3 times in water. Samples were incubated in 1% aqueous uranyl acetate for 1 h and followed by 2 washes in water and subsequent dehydration in grades of alcohol. The samples were then put in propylene oxide for 1 h and embedded in TAAB Epon. Ultrathin sections (about 60 nm) were cut on a Reichert Ultracut-S microtome, moved to copper grids, and then stained with lead citrate. Sections were examined in a JEOL 1200EX transmission electron microscope, and images were recorded with an AMT 2k CCD camera.

Uric acid measurement

To measure the uric acid (UA) content in whole flies, 5 flies were homogenized with 100 μL PBS containing 0.05% Tween 20 using multi-sample tissuelyser-24 (Shanghai Jingxin Technology). The supernatant was collected after centrifugation at 12,000 x *g* for 10 min at 4 °C. To measure the UA excretion, 20 flies were placed in an empty 1.5 mL EP tube for 1.5 h. The excretion was dissolved in 100 μL PBS. The UA amounts in the whole body and excretion were quantified using the Uric Acid Assay Kit (BioAssay Systems, DIUA-250) according to the manufacturer's instructions. Briefly, 5 μL of supernatant and UA standards were incubated with 200 μL assay buffer at room temperature (RT) for 30 min. The absorbance at 590 nm were measured in a plate reader.

Imaging of Malpighian tubule renal deposits

Adult Malpighian tubules were dissected in cold PBS. Intact Malpighian tubules were mounted on glass slides in cold PBS and were immediately imaged using a microscope (Nikon Eclipse Ts2).

Gut staining and fly appearances imaging

Adult midguts were dissected in PBS and fixed for 15 min in PBS containing 4% paraformaldehyde. After fixation, the samples were washed with PBS containing 0.2% Triton X-100 (PBST) and blocked with 1% BSA in PBST. Midguts were washed and then incubated with or without DAPI (1:1000, Thermo Fisher Scientific, D1306) for 15 min at RT, washed, and mounted in Vectashield (Vector, H-1000). Images of fly appearances were performed on a Nikon SMZ18 and confocal images of gut were obtained using a Zeiss LSM880.

Nanopore metagenome sequencing

To obtain bacterial genomic DNA (gDNA) from the fly intestines, whole midguts of 8 days old flies were maintained as intact tissues to prevent bacterial leakage, the crops and Malpighian tubules of fly guts were removed. 120 midguts were dissected from each sample and the gDNA was extracted using fecal DNA extracting kit (Tiangen, DP328). DNA libraries were constructed using the Oxford Nanopore Technologies (ONT) LSK109 library preparation kits following the manufacturer's instructions and were sequenced on single R9.4 flow cells on the Oxford Nanopore PromethION by Benagen (Wuhan, China). The raw signal data were basecalled using the ONT Albacore software package with default parameters. The reads were aligned to FlyBase genome annotation version r6.39 using minimap2 and Samtools to filter out *Drosophila* reads (control: 99.75%; yki^{3SA}: 96.1%). The final reads were bridged using Flye (v2.6) and racon (1.22) and annotated using Karken2 and Bracken. Three biological replicates were used to evaluate each genotype. We considered the species with >50 reads in more than two replicated as detected. A cut-off > 2-fold change consistently observed among replicates and the adjusted p value >0.05 from DSeq2 analysis were used. Metagenomic data were deposited in the Gene Expression Omnibus (GEO, GSE204975).

RNA-seq analysis of adult Malpighian tubules

80 Malpighian tubules were dissected for total RNA extraction. After assessing RNA quality with Agilent Bioanalyzer (RIN >7), mRNAs were enriched by poly-A pull-down. Sequencing libraries were prepared with Illumina Truseq RNA preparation kits and were sequenced using Illumina HiSeq 2000 by Benagen (Wuhan, China). We multiplexed samples in each lane, which yields target number of single-end 100-bp reads for each sample, as a fraction of 180 million reads for the whole lane. After trimming, sequence reads were mapped to the *Drosophila* genome (FlyBase genome annotation version r6.39) using Tophat. With the uniquely mapped reads, gene expression was quantified using Cufflinks (FPKM values) and HTseq (read counts per gene). RNA-seq data were deposited in the Gene Expression Omnibus (GEO, GSE204866).

Prior to fold change calculation, we set to a value of "1" for any FPKM value between 0 and 1 to reduce the possibility that we get large ratio values for genes with negligible levels of detected transcript in both the experimental sample and the wildtype control (e.g., FPKM 0.1 vs. 0.0001), as those ratios are unlikely to have biological relevance. A cut-off > 2-fold change and the adjusted p value <0.05 from DSeq2 analysis were used.

qPCR analysis of gene expression

A total of 10 adult midguts, 5 whole adult flies, 20 pairs of Malpighian tubules of each genotype were lysed with Trizol (Thermo Fisher Scientific, 15,596,018) for RNA extraction and cDNA was transcribed using HiScript II Q RT Supermix (Vazyme, R222-01). qPCR was

then performed using ChamQ SYBR qPCR Master Mix (Vazyme, Q311-03) on a CFX384 Real-Time System/C1000 Touch Thermal Cycler (Bio-Rad). *Drosophila* gene expression was normalized to *RpL32*.

Cell culture, constructs and luciferase assays

PGRP-SC2 fragment from fly cDNA and luciferase (Luci) fragment from pGL3-basic Luciferase Reporter Vector (Promega, E1751) were cloned into the pAc5.1 vector (Thermo Fisher Scientific, V411020) at EcoRI and XhoI sites using the exonuclease-based DNA assembly method (Vazyme, C113-01).

For luciferase assays, *Drosophila* S2R^{+} cells were seeded into a 12-well plate at 25 °C with Schneider's medium supplemented with 10% fetal bovine serum and antibiotics and then transfected with 300ng pAc5.1-PGRP-SC2-Luci and pAc5.1-Luci using the Effectene Transfection Reagent (Qiagen, 301,425). After 48h, conditioned medium and the remaining cells were collected for measurements of luciferase activities using the Dual-Luciferase Reporter Assay Reagent (Promega, E1910). Luciferase activities in the medium were normalized to intracellular luciferase activities. All of the results were obtained from at least three independent experiments.

Alamar blue cell viability assay

Mature PGRP-SC2 proteins (21-184aa) with a 6XHis tag at N terminus and a Myc tag at the C terminus was expressed in *E. coli* by CUSABIO (Wuhan, China) prior to affinity chromatography purification. Alamar blue cell viability assay was performed as described previously (Toda et al., 2019). A single colony of *E. coli* (Vazyme, C502), *Ecc15 and E. faecalis* (from Dr. Zongzhao Zhai), *S. typhimurium* and *M. luteus* (from Dr. Lei Pan), *S. aureus* (from Dr. Yingying Pu), *P. aeruginosa* (CCTCC, AB, 2010174), *P. putida* (CCTCC, AB, 2014017), *P. chlororaphis* (CCTCC, AB, 200053), *G. oxydans* (CCTCC, AB, 204035), *A gen.sp* (CCTCC, AB, 2012042T), *L. fermentum* (CCTCC, AB, 2015067), *L. plantarum* (CCTCC, AB, 2015024) were inoculated in 5 mL of culture medium at 200 rpm at 37 °C or 30 °C overnight. Bacterial cultures were diluted with PBS to OD_{600} = 0.05. 10 μL of diluted bacterial cultures were incubated with 80 μL PGRP-SC2 at different dosages or 50 ng/μL ampicillin (Amp) or kanamycin (Kan) in a 96-well plate at RT for 2 h. 10 μL of alamar blue (Thermo Fisher Scientific, DL1025) was added and incubated overnight at 37 °C or 30 °C. The quantification of bacterial amount was performed according to manufacturer's protocol.

Hemolymph PGN detection

Hemolymph was extracted from 50 decapitated female adults by centrifuging at 1,500 x *g* for 15 min at 4 °C and heated at 70 °C for 5 min. The supernatant was collected after centrifugation at 12,000 x *g* for 10 min at 4 °C. The concentration of hemolymph PGN was detected as described previously (Troha et al., 2019). 50 μL 1:10 diluted hemolymph was used for the SLP (Silkworm larvae plasma) assay (Fujifilm Wako Pure Chemical Corporation, 297–51501) following the manufacturer's instructions. For PGRP-SC2 amidase activity assay, 100 μL 1 mg/mL standard PGN were incubated with 80 μL of indicated final concentration of PGRP-SC2 proteins or 50 ng/μL kanamycin (Kan) at RT for 2h.

QUANTIFICATION AND STATISTICAL ANALYSIS

Data are presented as the mean ± SEM Unpaired Student's *t* test and one-way ANOVA followed by post-hoc test were performed to assess differences. The log rank tests were performed to assess significant differences in lifespan using the GraphPad Prism software. Measurements represent the mean of at least three biological replicates in all graphs. The *p value <0.05 was considered statistically significant.

Immunity, Volume *55*

Supplemental information

Renal NF-κB activation impairs uric acid homeostasis to promote tumor-associated mortality independent of wasting

Yuchen Chen, Wenhao Xu, Yuan Chen, Anxuan Han, Jiantao Song, Xiaoya Zhou, and Wei Song

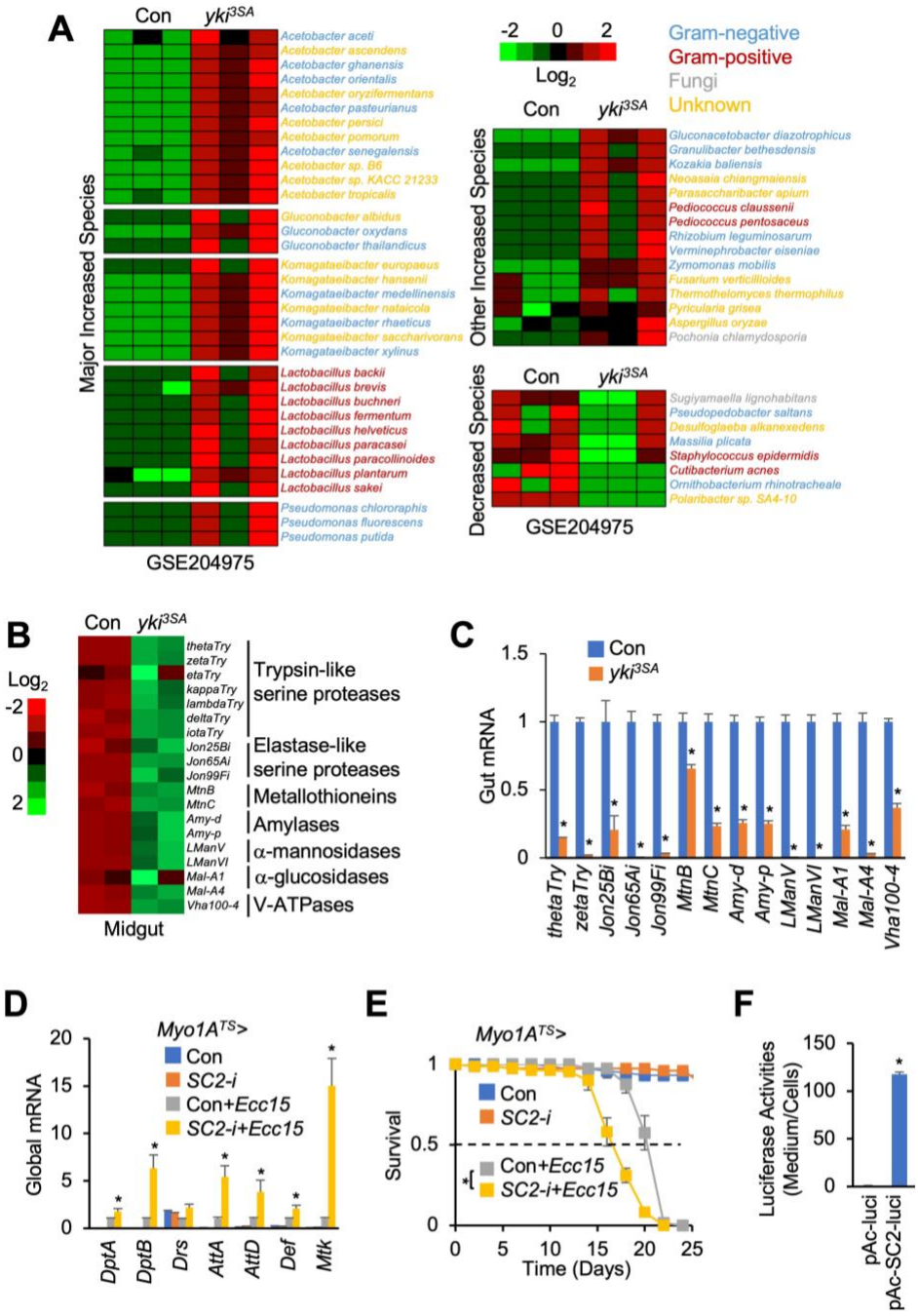

Supplemental Figure 1. Related to Figure 1 and Figure 3-4. Bacterial distribution in yki^{3SA}-tumor-bearing flies. (**A-C**) Heatmaps showing absolute abundance of gut microbial species (**A**), heatmap of RNAseq (**B**) and qPCR (**C,** n=4, 10 flies/replicates) data of gut gene expression in the control and yki^{3SA}-tumor flies under tumor induction using *GAL4* system for 8 days.

(**D**) qPCR analysis of gene expression in whole adult flies (n=6, 5 flies/replicate) bearing *PGRP-SC2* RNAi in the ECs with *Ecc15* infection for 8 days. (**E**) Lifespans of indicated flies (n=80) (Log-rank test; Con+*Ecc15* V.S. *SC2-i*+*Ecc15*, $P < 0.001$). (**F**) Ratios of luciferase activities in the medium to $S2R^+$ cell lysate (n=3). (**C**-**F**) Data are representative of at least three independent experiments. Data are presented as mean ± SEM. Student's t test, $*p < 0.05$. "ns" indicates statistically non-significant.

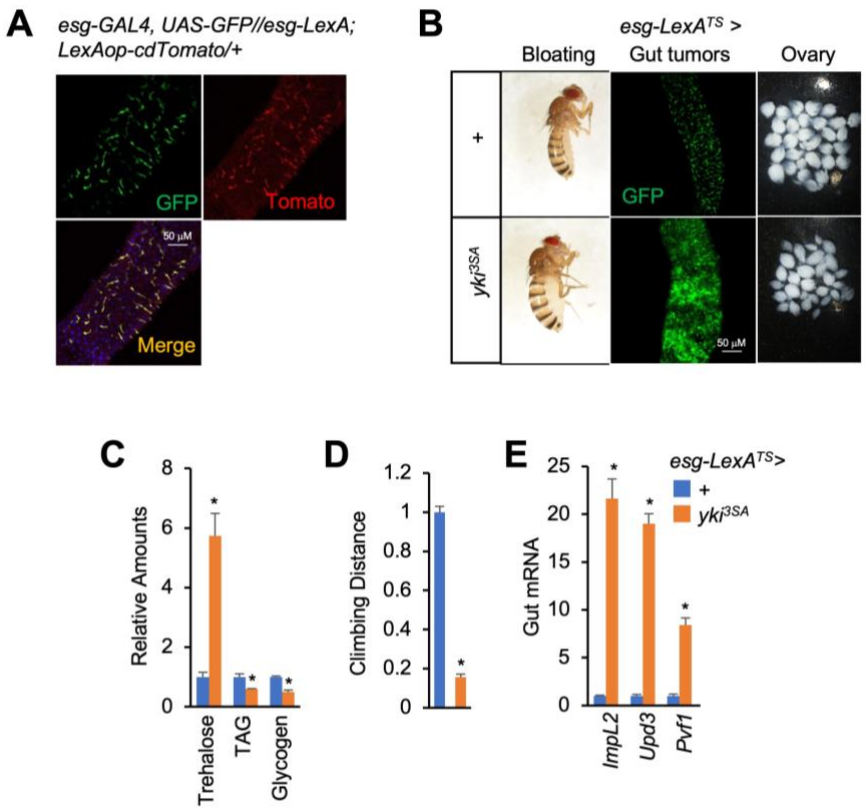

Supplemental Figure 2. Related to Figure 5. yki^{3SA}-tumor-bearing flies generated using *LexA* system. (**A**) Immunostaining indicating overlapping expression of *esg-GAL4, UAS-GFP* (green) and *esg-LexA, LexAop-cdTomato* (red) in the adult midgut. (**B-E**) Bloating phenotypes (left), gut tumors (middle, GFP) and ovary degeneration (right) (**B**), wasting effects such as TAG and trehalose amounts (**C**, n=3, 5 flies/replicate) and climbing defects (**D**, n=15), and qPCR analysis of cachectic ligand expression in the midgut (**E**, n=3, 10 flies/replicate) of flies under tumor induction using *LexA* system for 4 days. (**C-E**) Data are representative of at least three independent experiments. Data are presented as mean ± SEM. Student's t test, *$p < 0.05$.

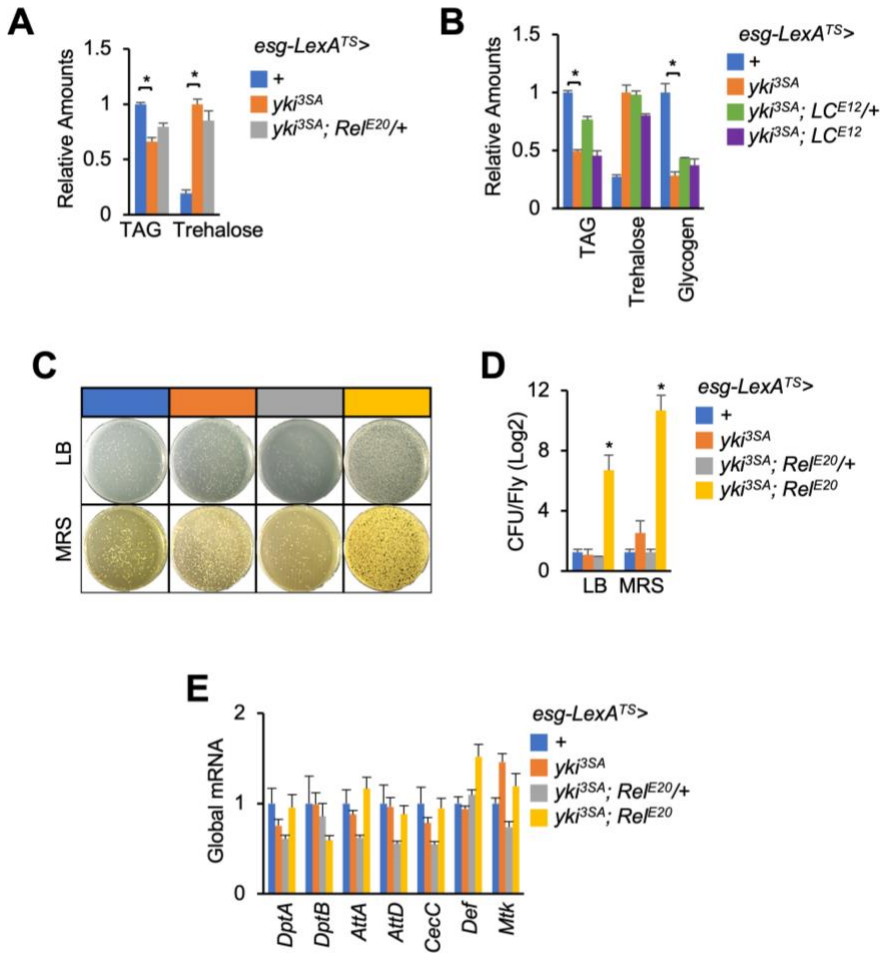

Supplemental Figure 3. Related to Figure 5. *Rel^{E20}*-null mutation causes bacterial overload at early adult stage. (**A-B**) Whole-body TAG, trehalose, and glycogen amounts (n=4, 5 flies/replicate) of flies under tumor-induction using *LexA* system in the context of *Rel^{E20}*/+ (**A**) and *PGRP-LC^{E12}* (**B**) mutation for 4 days. (**C-E**) Gut bacterial loads (**C**) and quantification (**D,** n=4, 5 flies/replicates) and qPCR analysis of whole-body gene expression (**E,** n=6, 5 flies/replicates) of flies under yki^{3SA}-induction using *LexA* system plus *Rel^{E20}* null-mutation for 1 day before tumor formation. Data are representative of at least three independent experiments. Data are presented as mean ± SEM. Student's t test, *$p < 0.05$.

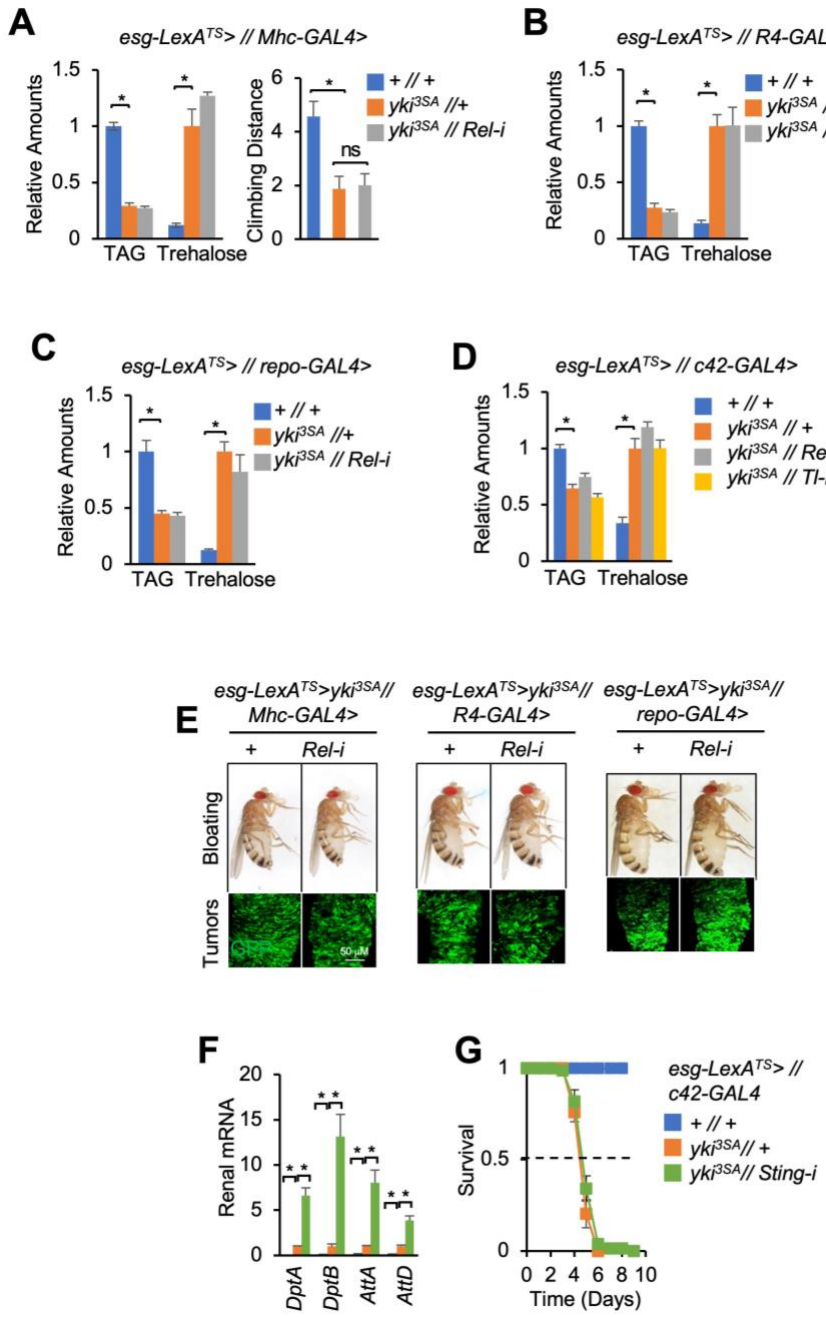

Supplemental Figure 4. Related to Figure 5. IMD-NF-κB blockade in multiple organs fails to improve tumor-induced wasting. (**A-E**) Whole-body TAG and trehalose amounts (n=4, 5 flies/replicate) and climbing rates (n=20) (**A-D**) and abdomen bloating and gut tumors (GFP) (**E**) of flies under tumor-induction using *LexA* system plus tissue-specific silencing of *Rel* using different *GAL4* lines for 4 days. (**F-G**) qPCR analysis of MT gene expression

at day 4 of tumor induction (**F**, n=4, 20 flies/replicate) and lifespan (**G,** n=80) of flies with yki^{3SA}-gut tumors using *LexA* system plus renal PC-specific *Sting* silencing using *c42-GAL4*. (**A-D**, and **F-G**) Data are representative of at least three independent experiments. Data are presented as mean ± SEM. Student's t test, *$p < 0.05$.

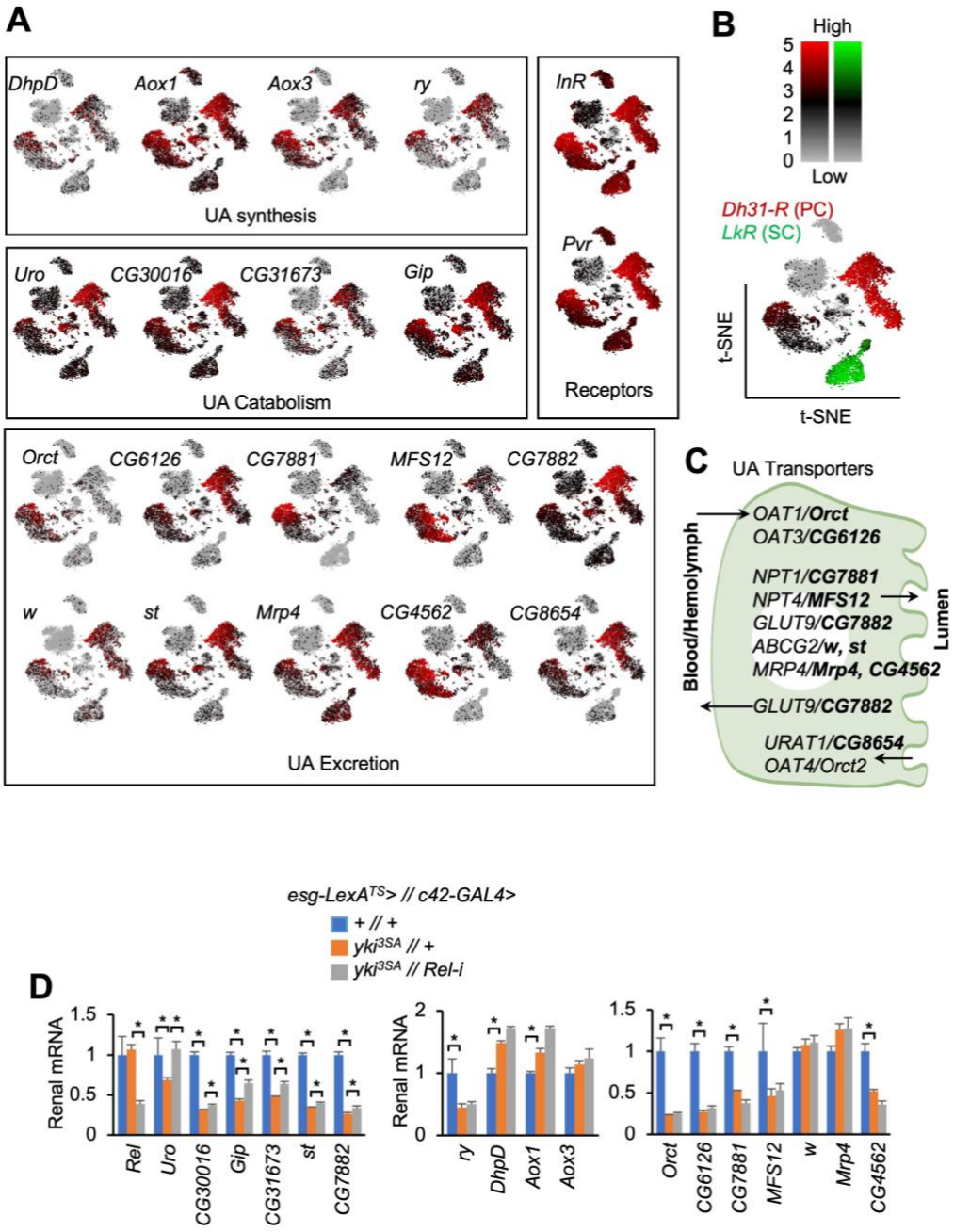

Supplemental Figure 5. Related to Figure 6. Single-cell RNAseq analysis of putative genes involved in UA metabolism. (**A**) Distributions of genes involved in UA synthesis, transport, and catabolism, as well as *InR* and *Pvr*, in the MT cells. (**B**) Two major PC clusters (*Dh31-R*$^{+}$, red) and one SC cluster (*LkR*$^{+}$, green) in adult MT (flycellatlas.org). (**C**) The schematic model of homologs mediating UA transport in mammals (left) and *Drosophila* (right). (**D**)

qPCR analysis of gene expression in the MTs of flies with yki^{3SA}-gut tumor induction using *LexA* system plus renal PC-specific *Rel* silencing using *c42-GAL4* for 4 days (n=4, 20 flies/replicates). (**D**) Data are representative of at least three independent experiments. Data are presented as mean ± SEM. Student's t test, *$p < 0.05$.

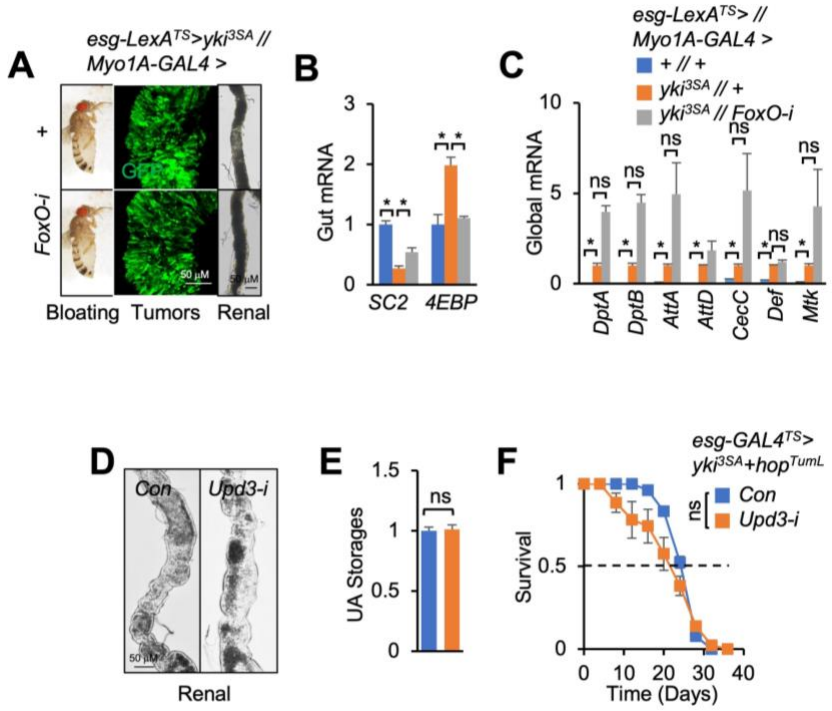

Supplemental Figure 6. Related to Figure 7. FoxO and Upd3 do not affect renal uric acid metabolism of yki^{3SA}-tumor-bearing flies. (**A-C**) Images showing abdomen bloating, gut tumors (GFP), and MT black deposits (**A**) and qPCR analysis of gene expression in the midgut (**B,** n=4, 10 flies/replicate) and whole body (**C,** n=6, 5 flies/replicate) of flies under yki^{3SA}-gut tumor induction using *LexA* system plus gut EC-specific *FoxO* silencing using *c42-GAL4* for 4 days. (**D-E**) Images showing MT black deposits (**D**) and whole-body uric acid amounts (**E**, n=4, 5 flies/replicate) of flies under induction of yki^{3SA}+hop^{TumL} tumors with or without *Upd3* silencing for 8 days using *GAL4* system. (**F**) Longevities of indicated flies (n=80) (Log-rank test, $P > 0.05$). Data are presented as mean ± SEM. *$p < 0.05$. (**B-C, and E-F**) Data are representative of at least three independent experiments. Data are presented

as mean ± SEM. Student's t test, *$p < 0.05$. "ns" indicates statistically non-significant.

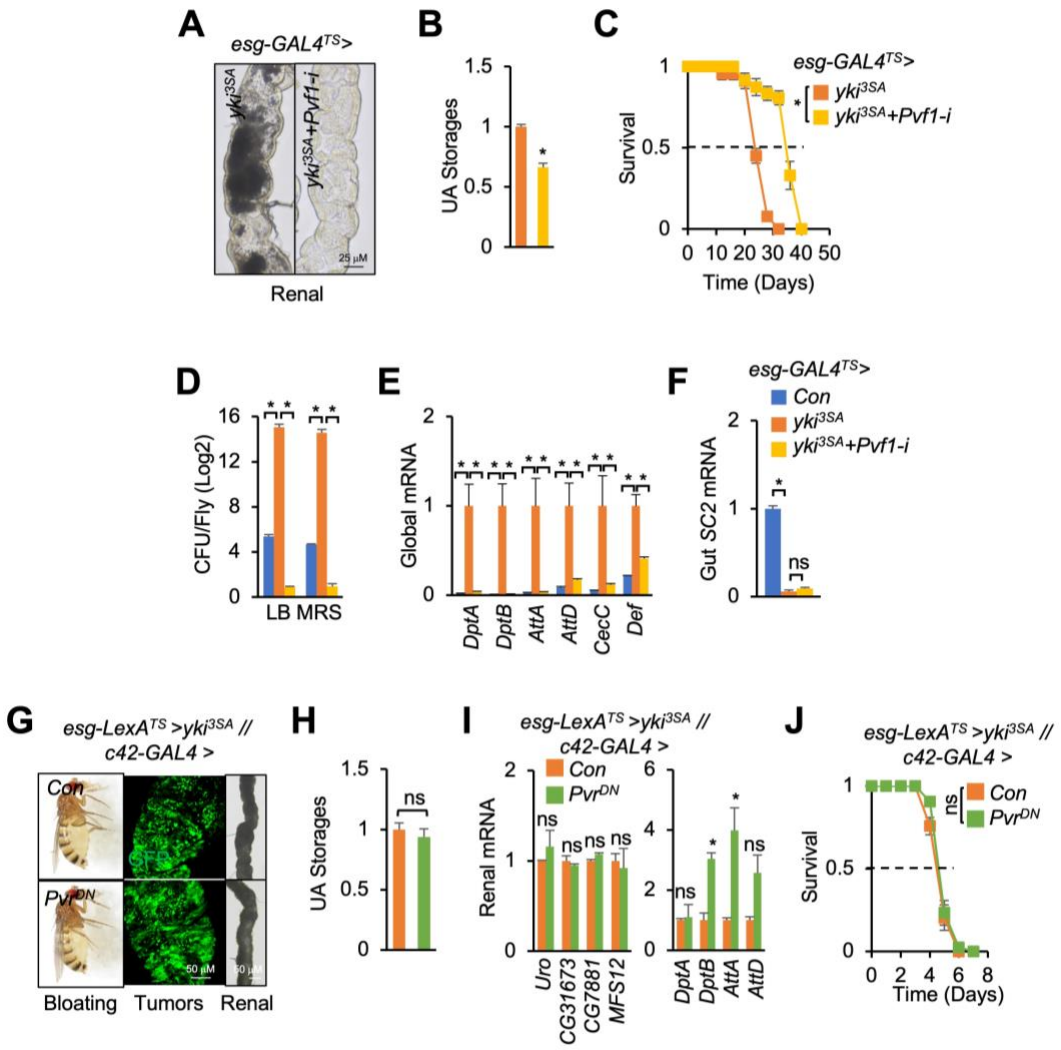

Supplemental Figure 7. Related to Figure 7. Tumor-derived Pvf1 impairs gut bacterial homeostasis and renal UA metabolism. (**A-F**) Images showing MT black deposits (**A**), whole-body uric acid amounts (**B**, n=4, 5 flies/replicate), quantification of gut bacterial loads (**D**, n=4, 5 flies/replicate), whole body (**E,** n=6, 5 flies/replicate) and midgut (**F**, n=4, 10 flies/replicate) gene expression indicated by qPCR of flies under induction of yki^{3SA} tumors with or without *Pvf1* silencing for 8 days using *GAL4* system. (**C**) Longevities of indicated flies (n=80) (Log-rank test, *yki^{3SA}* V.S. *yki^{3SA}+Pvf1-i*, $P < 0.001$).

(**G-J**) Images showing abdomen bloating, gut tumors (green), and MT black deposits (**G**), whole-body uric acid amounts (**H**, n=4, 5 flies/replicate), and renal gene expression (**I,** n=4, 20 flies/replicate) flies under yki^{3SA}-gut tumor induction using *LexA* system plus MT PC-specific *Pvr^{DN}* overexpression using *c42-GAL4* for 4 days. (**J**) Longevities of indicated flies (n=80) (Log-rank test, *Con* V.S. *Pvr^{DN}*, $p > 0.05$, ns). Data are presented as mean ± SEM. *$p < 0.05$. (**B-F**, and **H-J**) Data are representative of at least three independent experiments. Data are presented as mean ± SEM. Student's t test, *$p < 0.05$. "ns" indicates statistically non-significant.

Supplemental Table S5: DNA primer information. Related to STAR Methods.

qPCR primers

Genes	Sequence
RpL32-F	GCTAAGCTGTCGCACAAATG
RpL32-R	GTTCGATCCGTAACCGATGT
PGRP-LC-F	CACGCAGGGTATTGGCAGCATC
PGRP-LC-R	CCTCGCCCCGGTTTCCACTTG
PGRP-LE-F	GATGCCGACCAAAATACCAG
PGRP-LE-R	GTCTTCGAAATGTGTCGGAG
PGRP-LB-F	GCTCATGCACCCAAGTACAA
PGRP-LB-R	GGGTCAATGTAGCCCTTGAA
PGRP-SC2-F	TGGCAAACAAAGCTCTCATC
PGRP-SC2-R	ACGGCGTAGCTCAGGTAGTT
PGRP-SC1a/b-F	CTATGTCGTCTCCAAGGCGGAGT
PGRP-SC1a/b-R	CGATCAGGAAGTTGTAGCCGATGT
PGRP-SB1-F	TCGTCTTCATTGGCAACTTC
PGRP-SB1-R	GATGACCGAACAGCGTGTAG
PGRP-SB2-F	ACTATTCCGTGGTGGGTCAT
PGRP-SB2-R	TTGAGCTCGTTGAGAAGGTG
DptA-F	GCTGCGCAATCGCTTCTACT
DptA-R	TGGTGGAGTGGGCTTCATG
DptB-F	AGCCTGAACCACTGGCATA
DptB-R	AGATCGAATCCTTGCTTTGG
Drs-F	ACCAAGCTCCGTGAGAACCTT
Drs-R	TTGTATCTTCCGGACAGGCAG
AttA-F	TACTCCCACATCAACGGACA
AttA-R	TCCCGTGAGATCCAAGGTAG
AttD-F	GTCACTAGGGTTCCTCAG
AttD-R	GCCGAAATCGGACTTG
Mtk-F	CCACCGAGCTAAGATGCAA
Mtk-R	GCTCTGCCAGCACTGATGTA
Def-F	GAGCCACATGCGACCTACTC
Def-R	CAGTAGCCGCCTTTGAACC
CecA-F	TCTTCGTTTTCGTCGCTCTCA
CecA-R	ATTCCCAGTCCCTGGATTGTG

CecC-F	TCATCCTGGCCATCAGCATT
CecC-R	CGCAATTCCCAGTCCTTGAAT
PGRP-SD-F	GGAAGTACCGATCGTGACGAGG
PGRP-SD-R	CTTGGTAGCACTGACTTGACGATGG
ImpL2-F	AAGAGCCGTGGACCTGGTA
ImpL2-R	TTGGTGAACTTGAGCCAGTCG
4EBP-F	CTCCTGGAGGCACCAAACTTATC
4EBP-R	TTCCCCTCAGCAAGCAACTG
Pvf1-F	CTGTCCGTGTCCGCTGAG
Pvf1-R	CTCGCCGGACACATCGTAG
Upd3-F	CTGGTCACTGATCTTACTCGCC
Upd3-R	GGATTGGTGGGATTGATGGGA
Relish-F	AGACAGAGCGTGAGGCCAAG
Relish-R	GACGATGCGAAGCTCTCCAG
Rosy-F	TGGTGACTTCCCACTGGAG
Rosy-R	GGTTCGGGTATTTCAAGCAG
DhpD-F	GCAACCGTGTTTCTTGGAACT
DhpD -R	CCACTGCCAGGAATCCTCC
Aox1-F	TTTGGAGGCAACATCTGTCG
Aox1-R	GGGACACTTTTTGGTGCTCAG
Aox3-F	CTGCCCTATGCAGTGAATCTAAC
Aox3-R	GGCACGAATTGACAGCCCA
Uro-F	GACTTCAGCTCCATTGACAAC
Uro-R	GAGACCCTTGATGCCCG
Gip-F	TAGAGATCCCCTATCCCGAAGG
Gip-R	ATTGGCTACGGAACAGCTTTT
CG31673-F	TGCTGATTTCGCATCCAAATGT
CG31673-R	GCAGATGATGGTCTCCGCT
CG30016-F	GATGCACGAAAGTTTTCTACCC
CG30016-R	GGGATCTCCATTCCTGAATCT
CG6126-F	TACTGGAGGACCTGATGGGG
CG6126-R	CAGGACTCTAGCTCGCCATT
Orct-F	CTGGTGCTTCAGCTAATCTTCG
Orct-R	GCCCACAATCATACGGGAAATC
St-F	CACACCCAAGCTATCGAAACG
St-R	GTGGGCGACCATTTGCTGTA

CG7881-F	GGATGCGGCCACTACTAACTT
CG7881-R	AGCTGGACAGAATGTATGATTGC
w-F	GCCTGGCACAATATGGACATC
w-R	GTTGCAGAATAGTCCGCGTGT
Mrp4-F	AAACTCCACGTTTGGGTCG
Mrp4-R	CAAGCAGGAATACTCCCGTAATG
CG7882-F	ATTGCCAGCTATGACCTGAAC
CG7882-R	CGCCTCCAACGAGGAATATGG
MFS12-F	AAGTCCCTGATCCTCAGCAG
MFS12-R	AACTTGGCTCCAAATCGCTTG
CG4562-F	ACAGGAGCACAGATCAGATCA
CG4562-R	TCCAAGATGAAGAGGACCAGG

Cloning Primers

Primer name	**Sequence**
pUAST-PGRP-SC1-F	TAGTCCAGTGTGGTGGAATTATGGTTTCCAAAGTGGCTC
pUAST-PGRP-SC1-R	GCTCTAGATTACGTAGAATCGAGACCGAGGAGAGGG
pJFRC19-13XLexAop2-yki^{3SA}-F	CCGCTCGAGATGTGCGCGTGCCTAATCGC
pJFRC19-13XLexAop2-yki^{3SA}-R	GCTCTAGATTACGTAGAATCGAGACCGAGGAGAGGG
pAc5.1-PGRP-SC2-Luci-F	ACTAGTCCAGTGTGGTGGATGGCAAACAAAGCTCTC
pAc5.1-PGRP-SC2-Luci-R	GTTTTTGGCGTCTTCCATGGCCTTCCAGTTGGACCAG
pAc5.1-Luci-F	TACTAGTCCAGTGTGGTGGAATTCATGGAAGACGCCAAAAACATAAAG
pAc5.1-Luci-R	CTGTGCTGGATATCTGCAGAATTCTTACACGGCGATCTTTCCGCCCTTCTT